

# Effective interactions for the nuclear shell model

M. Hjorth-Jensen<sup>a,b</sup>

<sup>a</sup> *NORDITA, Blegdamsvej 17, DK-2100 København Ø, Denmark*

<sup>b</sup> *Department of Physics, University of Oslo, N-0316 Oslo, Norway*

---

## Abstract

Various perturbative and non-perturbative many-body techniques are discussed in this work. Especially, we will focus on the summation of so-called Parquet diagrams with emphasis on applications to finite nuclei. Here, the subset of two-body Parquet equations will be discussed. A practical implementation of the corresponding equations for studies of effective interactions for finite nuclei is outlined.

*Keywords:* Many-body theory, effective interactions, shell model

---

## Contents

|     |  |    |
|-----|--|----|
| 1   | Introduction   | 2  |
| 2   | Perturbative methods   | 5  |
| 2.1 | Expressions for the wave operator  | 7  |
| 3   | Summation of diagrams in the [12] channel  | 11 |
| 3.1 | The $G$ -matrix  | 14 |
| 3.2 | Folded diagrams and the effective valence space interaction                                    | 20 |
| 3.3 | Selected applications  | 26 |
| 3.4 | Inclusion of hole-hole contributions and single-particle propagators                           | 32 |
| 4   | Screening corrections and vertex renormalization, the equations for the [13] and [14] channels | 35 |
| 4.1 | Screened ph and 2p2h interactions  | 38 |
| 4.2 | Further renormalizations   | 43 |
| 5   | Effective interactions for finite nuclei from Parquet diagrams                                 | 45 |
| 5.1 | Petit Parquet  | 47 |
| 6   | Perspectives   | 49 |
|     | References   | 51 |

## 1 Introduction

Traditional shell-model studies have recently received a renewed interest through large scale shell model calculations in both the  $1p0f$  shell and the  $2s1d0g_{7/2}$  shells with the inclusion of the  $0h_{11/2}$  intruder state as well. It is now therefore fully possible to perform large-scale shell-model investigations and study the excitation spectra for systems with some 10 million basis states. With recent advances in Monte Carlo methods one is also able to enlarge the dimensionality of the systems under study considerably, and important information on e.g., ground state properties has thereby been obtained.

An important feature of such large scale calculations is that it allows one to probe the underlying many-body physics in a hitherto unprecedented way. The crucial starting point in all such shell-model calculations is the derivation of an effective interaction, be it either an approach based on a microscopic theory starting from the free nucleon-nucleon ( $NN$ ) interaction or a more phenomenologically determined interaction. In shell-model studies of e.g., the Sn isotopes, one may have up to 31 valence particles or holes interacting via e.g., an effective two-body interaction. The results of such calculations can therefore yield, when compared with the available body of experimental data, critical inputs to the underlying theory of the effective interaction. Until very recently, realistic shell-model effective interactions have mainly been applied to nuclei with two or a few valence particles beyond closed shells, such as the oxygen and calcium isotopes. Thus, by going to the tin isotopes, in which the major neutron shell between neutron numbers 50 and 82 is being filled beyond the  $^{100}\text{Sn}$  closed shell core, we have the opportunity of testing the potential of large-scale shell-model calculations as well as the reliability of realistic effective interactions in systems with many valence particles.

Clearly, although the  $NN$  interaction is of short but finite range, with typical interparticle distances of the order of  $1 \sim 2$  fm, there are indications from both studies of few-body systems such as the triton and infinite nuclear matter, that at least three-body interactions, both real and effective ones, may be of importance. Thus, with many valence nucleons present, such large-scale shell-model calculations may tell us how well e.g., an effective interaction which only includes two-body terms does in reproducing properties such as excitation spectra and binding energies.

This work deals therefore with various ways of deriving the effective interaction or effective operator needed in shell-model calculations, starting from the free  $NN$  interaction. Normally, the problem of deriving such effective operators and interactions are solved in a limited space, the so-called model space, which is a subspace of the full Hilbert space. The effective operator and interaction theory is then introduced in order to systematically take into account contributions from the complement (the excluded space) of the chosen model space. Several formulations for such expansions of effective operators and interactions exist in the literature, following time-dependent or time-independent perturbation theory [1–6]. Formulations like the coupled-cluster method or exponential ansatz [5,7–13], the summation of the Parquet class of diagrams [14–21], or the so-called  $\hat{Q}$ -box method with the folded-diagram formulation of Kuo and co-workers [3,4] have been extensively applied to systems in nuclear, atomic, molecular and solid-state physics. Here we will focus on the above-mentioned  $\hat{Q}$ -box approach and the summation of the so-called Parquet diagrams. For the description of other many-body methods such as the Hypernetted-chain or the correlated basis function [22] methods, monte-carlo related methods [23,24], Unitary-correlation operator method [6] etc. see other contributions in this volume.

The  $\hat{Q}$ -box has been introduced in Rayleigh-Schrödinger perturbation theory as the definition of all non-folded diagrams to a given order in the expansion parameter, in nuclear

physics the so-called  $G$ -matrix. The  $G$ -matrix renders the free  $NN$  interaction  $V$ , which is repulsive at small internucleon distances, tractable for a perturbative analysis through the summation of ladders diagrams to infinite order. Stated differently, the  $G$ -matrix, through the solution of the Bethe-Brueckner-Goldstone equation, accounts for the short-range correlations involving high-lying states. Folded diagrams are a class of diagrams which arise due to the removal of the dependence of the exact model-space energy in the Brillouin-Wigner perturbation expansion. Through the  $\hat{Q}$ -box formulation and its derivatives, this set of diagrams can easily be summed up.

In addition to the evaluation of folded diagrams and the inclusion of ladder diagrams to infinite order included in the  $G$ -matrix, there are other classes of diagrams which can be summed up. These take into account the effect of long-range correlations involving low-energy excitations. A frequently applied formalism is the Tamm-Dancoff (TDA) or the random-phase (RPA) approximations. In their traditional formulation one allows for the summation of all particle-hole excitations, both forward-going and backward going insertions. This set of diagrams, as formulated by Kirson [25] and reviewed in Ref. [26], should account for correlations arising from collective particle-hole correlations. Another possibility, is to include any number of particle-particle and hole-hole correlations in the screening of particle-hole correlations. The inclusion of these kind of correlations is conventionally labelled particle-particle (pp) RPA. It has been used both in nuclear matter studies [27–30] and in evaluations of ground state properties of closed-shell nuclei [31–33]. Recently, Ellis, Mavromatis and Müther [32,33] have extended the pp RPA to include the particle-hole (ph) RPA, though screening of two-particle-one-hole (2p1h) and two-hole-one-particle (2h1p) vertices was not included. The latter works can be viewed as a step towards the full summation of the Parquet class of diagrams. The summation of the Parquet diagrams entails a self-consistent summation of both particle-particle and hole-hole ladder diagrams and particle-hole diagrams. Practical solutions to this many-body scheme for finite nuclei will be discussed here.

This work falls in six sections. In the next section we present various definitions pertinent to the determination of effective interactions, with an emphasis on perturbative methods. The resummation of the ladder type of diagrams is then presented in section 3. In that section we also discuss the summation of so-called folded diagrams which arise in the evaluation of valence space effective interactions. Further perturbative corrections are also discussed and selected results for light nuclei in the  $1s0d$  and  $1p0f$  shells and for Sn isotopes are presented.

The summation of the TDA and RPA class of diagrams is discussed in section 4. Other screening corrections are also discussed in that section. The self-consistent approach to the summation of both ladder type diagrams and screening terms through the solution of equations for the Parquet class of diagrams will be presented in section 5. Concluding remarks are given in section 6.

## 2 Perturbative methods

In order to derive a microscopic approach to the effective interaction and/or operator within the framework of perturbation theory, we need to introduce various notations and definitions pertinent to the methods exposed. In this section we review how to calculate an effective operator within the framework of degenerate Rayleigh-Schrödinger (RS) perturbation theory [3,5].

It is common practice in perturbation theory to reduce the infinitely many degrees of freedom of the Hilbert space to those represented by a physically motivated subspace, the model space. In such truncations of the Hilbert space, the notions of a projection operator  $P$  onto the model space and its complement  $Q$  are introduced. The projection operators defining the model and excluded spaces are defined by

$$P = \sum_{i=1}^D |\Phi_i\rangle \langle \Phi_i|, \quad (1)$$

and

$$Q = \sum_{i=D+1}^{\infty} |\Phi_i\rangle \langle \Phi_i|, \quad (2)$$

with  $D$  being the dimension of the model space, and  $PQ = 0$ ,  $P^2 = P$ ,  $Q^2 = Q$  and  $P + Q = I$ . The wave functions  $|\Phi_i\rangle$  are eigenfunctions of the unperturbed hamiltonian  $H_0 = T + U$ , where  $T$  is the kinetic energy and  $U$  an appropriately chosen one-body potential, that of the harmonic oscillator (h.o.) in most calculations. The full hamiltonian is then rewritten as  $H = H_0 + H_1$  with  $H_1 = V - U$ ,  $V$  being e.g. the  $NN$  interaction. The eigenvalues and eigenfunctions of the full hamiltonian are denoted by  $|\Psi_\alpha\rangle$  and  $E_\alpha$ ,

$$H |\Psi_\alpha\rangle = E_\alpha |\Psi_\alpha\rangle. \quad (3)$$

Rather than solving the full Schrödinger equation above, we define an effective hamiltonian acting within the model space such that

$$PH_{\text{eff}}P |\Psi_\alpha\rangle = E_\alpha P |\Psi_\alpha\rangle = E_\alpha |\Phi_\alpha\rangle \quad (4)$$

where  $|\Phi_\alpha\rangle = P |\Psi_\alpha\rangle$  is the projection of the full wave function onto the model space, the model space wave function. In RS perturbation theory, the effective interaction  $H_{\text{eff}}$  can be written out order by order in the interaction  $H_1$  as

$$PH_{\text{eff}}P = PH_1P + PH_1 \frac{Q}{e} H_1 P + PH_1 \frac{Q}{e} H_1 \frac{Q}{e} H_1 P + \dots, \quad (5)$$

where terms of third and higher order also include the aforementioned folded diagrams. Further,  $e = \omega - H_0$ , where  $\omega$  is the so-called starting energy, defined as the unperturbed

energy of the interacting particles.. Similarly, the exact wave function  $|\Psi_\alpha\rangle$  can now be written in terms of the model space wave function as

$$|\Psi_\alpha\rangle = |\Phi_\alpha\rangle + \frac{Q}{e}H_1|\Phi_\alpha\rangle + \frac{Q}{e}H_1\frac{Q}{e}H_1|\Phi_\alpha\rangle + \dots \quad (6)$$

The wave operator is often expressed as

$$\Omega = 1 + \chi, \quad (7)$$

where  $\chi$  is known as the correlation operator. The correlation operator generates the component of the wave function in the  $Q$ -space and must therefore contain at least one perturbation. Observing that  $P\Omega P = P$ , we see that the correlation operator  $\chi$  has the properties

$$P\chi P = 0, \quad Q\Omega P = Q\chi P = \chi P. \quad (8)$$

Since  $|\Psi_i\rangle = \Omega|\Psi_i^M\rangle$  determines the wave operator only when it operates to the right on the model space, i.e., only the  $\Omega P$  part is defined, the term  $\Omega Q$  never appears in the theory, and we could therefore add the conditions  $Q\chi Q = 0$  and  $P\chi Q = 0$  to Eq. (8). This leads to the following choice for  $\chi$

$$\chi = Q\chi P. \quad (9)$$

This has been the traditional choice in perturbation theory [1,5].

The wave operator  $\Omega$  can then be ordered in terms of the number of interactions with the perturbation  $H_1$

$$\Omega = 1 + \Omega^{(1)} + \Omega^{(2)} + \dots, \quad (10)$$

where  $\Omega^{(n)}$  means that we have  $n$   $H_1$  terms. Explicitly, the above equation reads

$$\begin{aligned} \Omega|\Phi_i\rangle = & |\Phi_i\rangle + \sum_\alpha \frac{|\alpha\rangle\langle\alpha|V|\Phi_i\rangle}{\varepsilon_i - \varepsilon_\alpha} + \sum_{\alpha\beta} \frac{|\alpha\rangle\langle\alpha|V|\beta\rangle\langle\beta|V|\Phi_i\rangle}{(\varepsilon_i - \varepsilon_\alpha)(\varepsilon_i - \varepsilon_\beta)} \\ & - \sum_{\alpha j} \frac{|\alpha\rangle\langle\alpha|V|\Phi_j\rangle\langle\Phi_j|V|\Phi_i\rangle}{(\varepsilon_i - \varepsilon_\alpha)(\varepsilon_i - \varepsilon_j)} + \dots, \end{aligned} \quad (11)$$

where  $\varepsilon$  are the unperturbed energies of the  $P$ -space and  $Q$ -space states defined by  $H_0$ . The greek letters refer to  $Q$ -space states, whereas a latin letter refers to model-space states. The second term in the above equation corresponds to  $\Omega^{(1)}$  while the third and fourth define  $\Omega^{(2)}$ . Note that the fourth term diverges in case we have a degenerate or nearly degenerate model space. It is actually divergencies like these which are to be removed by the folded diagram procedure to be discussed in the next section. Terms like these arise due to the introduction of an energy independent perturbative expansion. Conventionally, the various contributions

to the perturbative expansion are represented by Feynman-Goldstone diagrams. In Fig. 1 we display the topologically distinct contributions to first order in the interaction  $V$  to the wave operator Eq. (12). These diagrams all define the correlation operator  $\chi$  to first order in  $V$ . Diagrams with Hartree-Fock contributions and single-particle potential terms are not included. The possible renormalizations of these diagrams will be discussed in the next three sections. The reader should note that with respect to the nomenclature in Eq. (12), we will hereafter employ the following notation in our discussion of various diagrams and vertex renormalizations:

- roman letters  $p, q, r, s, t, \dots$  refer to particle single-particle states, either within the model-space or from the excluded space. An arrow pointing upwards represents such a particle state.
- greek letters  $\alpha, \beta, \gamma, \delta \dots$  refer to hole single-particle states. An arrow pointing downward is a hole state.

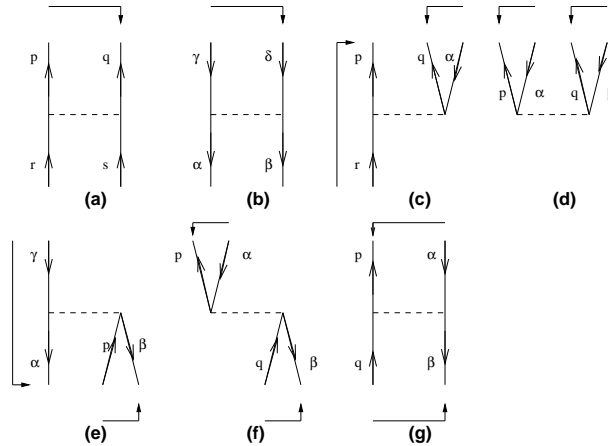


Fig. 1. The various vertices to first order in the interaction  $V$  which contribute to the wave operator  $\Omega = 1 + \chi$ . Hartree-Fock terms are not included. Possible hermitian conjugate diagrams are also not shown. Indicated are also possible angular momentum coupling orders.

## 2.1 Expressions for the wave operator

We end this section with the equations for the diagrams in Fig. 1 representing  $\chi$  to first order in  $V$ . Moreover, in order to introduce the various channels needed to sum the Parquet class of diagrams, we will find it convenient here to classify these channels in terms of angular momentum recouplings. Later on, we will also introduce the pertinent definitions of energy and momentum variables in the various channels. The nomenclature we will follow in our labelling is that of Blaizot and Ripka, see Ref. [18] chapter 15. All matrix elements in the definitions below are antisymmetrized and unnormalized. The first channel is the [12] channel, or the  $s$ -channel in field theory, and its angular momentum coupling order is depicted in Fig. 2. In this figure we do not distinguish between particles and holes, all

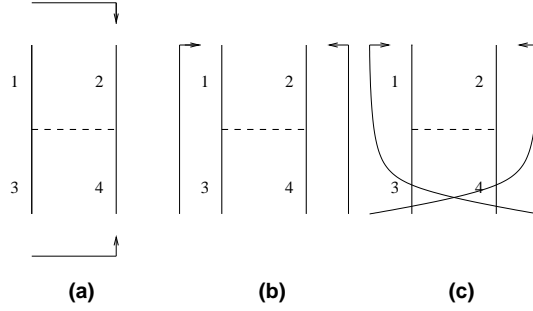


Fig. 2. Coupling order for the [12] (a), [13] (b) and [14] (c) channels.

single-particle labels 1, 2, 3, 4 can represent either a hole or particle single-particle state. It is the coupling order which is of interest here. The matrix element  $V^{[12]}$  in the [12] channel is then

$$V_{1234J}^{[12]} = \langle (12)J | V | (34)J \rangle, \quad (12)$$

meaning that the single-particle state 1(3) couples to the state 2(4) to yield a total angular momentum  $J$ . This channel is commonly denoted as the particle-particle (pp) or particle-particle-hole-hole (pphh) channel, meaning that when we will sum classes of diagrams to infinite order in this channel, the only intermediate states which are allowed are those of a pphh character, coupled to a final  $J$  in the above order. In the next section we will explicitly discuss ways to evaluate the equations for the [12] channel. This coupling order is also the standard way of representing effective interactions for shell-model calculations. If we now specialize to particles and holes (these matrix elements were shown in Fig. 1) we obtain for the case with particle states only, diagram (a),

$$V_{2p} = V_{pqrsJ}^{[12]} = \langle (pq)J | V | (rs)J \rangle. \quad (13)$$

The corresponding one for holes only, diagram (b), is

$$V_{2h} = V_{\alpha\beta\gamma\delta J}^{[12]} = \langle (\alpha\beta)J | V | (\gamma\delta)J \rangle. \quad (14)$$

Thus, in the forthcoming discussion, we will always employ as our basic notation for a matrix element that of the [12] channel, meaning that matrix elements of the other two channels can always be rewritten in terms of those in [12] channel. We see this immediately by looking at the expression for the matrix element in the [13] channel, the  $t$ -channel in field theory, see Fig. 2(b). Here the single-particle state 3(4) couples to the single-particle state 1(2)<sup>1</sup>. Through simple angular momentum algebra we have

$$V_{1234J}^{[13]} = \sum_{J'} (-)^{j_1+j_4+J+J'} \hat{j}_J'^2 \left\{ \begin{matrix} j_3 & j_1 & J \\ j_2 & j_4 & J' \end{matrix} \right\} V_{1234J}^{[12]}, \quad (15)$$

<sup>1</sup>In a Goldstone-Feynman diagram in an angular momentum representation, the coupling direction will always be from incoming single-particle states to outgoing single-particle states.

where the symbol with curly brackets represents a  $6j$ -symbol and  $\hat{J}' = \sqrt{2J'+1}$ . In a similar way we can also express the matrix element in the [14] channel, the  $u$ -channel in field theory, through

$$V_{1234J}^{[14]} = \sum_{J'} (-)^{j_1+j_4+J+2j_3} \hat{J}'^2 \left\{ \begin{matrix} j_4 & j_1 & J \\ j_2 & j_3 & J' \end{matrix} \right\} V_{1234J}^{[12]}. \quad (16)$$

It is also possible to have the inverse relations or to express e.g., the [14] channel through the [13] channel as

$$V_{1234J}^{[14]} = \sum_{J'} (-)^{2j_1+2j_2+2j_3} \hat{J}'^2 \left\{ \begin{matrix} j_4 & j_1 & J \\ j_3 & j_2 & J' \end{matrix} \right\} V_{1234J}^{[13]}. \quad (17)$$

The matrix elements defined in Eqs. (12)-(17) and the inverse relations are the starting points for various resummation of diagrams. In the next section we will detail ways of solving equations in the [12] channel, whereas various approximations for the [13] channel and [14] channel such as the TDA and RPA and vertex and propagator renormalization schemes will be discussed in section 4. Finally, how to merge self-consistently all three channels will be discussed in section 5.

We end this section by giving the expressions in an angular momentum basis<sup>2</sup> for the remaining diagrams of Fig. 1. The coupling order is indicated in the same figure.

Thus, the 2p1h vertex  $V_{2p1h}$ , diagram (c) in Fig. 1, is coupled following the prescription of the [13] channel and reads

$$V_{2p1h} = V_{pqr\alpha J}^{[13]} = \sum_{J'} (-)^{j_\alpha+j_p+J+J'} \hat{J}'^2 \left\{ \begin{matrix} j_r & j_p & J \\ j_q & j_\alpha & J' \end{matrix} \right\} V_{pqr\alpha J'}^{[12]}. \quad (18)$$

The 2p2h ground-state correlation  $V_{2p2h}$ , diagram (d), which will enter in the RPA summation discussed in section 4 is given by, the coupling order is that of the [13] channel,

$$V_{2p2h} = V_{pq\alpha\beta J}^{[13]} = \sum_{J'} (-)^{j_\beta+j_p+J+J'} \hat{J}'^2 \left\{ \begin{matrix} j_\alpha & j_p & J \\ j_q & j_\beta & J' \end{matrix} \right\} V_{pq\alpha\beta J'}^{[12]}. \quad (19)$$

---

<sup>2</sup>Note that we only include angular momentum factors, other factors coming from the diagram rules[34], like number of hole lines, number of closed loops etc. are omitted here.

The 2h1p vertex  $V_{2h1p}$ , diagram (e), still in the representation of the [13] channel, is defined as

$$V_{2h1p} = V_{\alpha\beta\gamma p J}^{[13]} = \sum_{J'} (-)^{j_\alpha + j_p + J + J'} \hat{J}'^2 \left\{ \begin{array}{ccc} j_\gamma & j_\alpha & J \\ j_\beta & j_p & J' \end{array} \right\} V_{\alpha\beta\gamma p J'}^{[12]}. \quad (20)$$

Note well that the vertices of Eqs. (18)-(20) and their respective hermitian conjugates can all be expressed in the [14] channel or [12] channel as well. However, it is important to note that the expressions in the various channels are different, and when solving the equations for the various channels, the renormalizations will be different. As an example, consider the two particle-hole vertices  $V_{ph}$  of Fig. 1, i.e., diagrams (f) and (g). Diagram (g) is just the exchange diagram of (f) when seen in the [12] channel. However, if (f) is coupled as in the [13] channel, recoupling this diagram to the [14] channel will not give two particle-hole two-body states coupled to a final  $J$  but rather a particle-particle two-body state and a hole-hole two-body state. But why bother at all about such petty details? The problem arises when we are to sum diagrams in the [13] channel and [14] channel. In the [12] channel we allow only particle-particle and hole-hole intermediate states, whereas in the [13] channel and [14] channel we allow only particle-hole intermediate states, else we may risk to double-count various contributions. If we therefore recouple diagram (f) to the [14] representation, this contribution does not yield an intermediate particle-hole state in the [14] channel. Thus, diagram (f), whose expression is

$$V_{ph} = V_{p\beta\alpha q J}^{[13]} = \sum_{J'} (-)^{j_p + j_q + J + J'} \hat{J}'^2 \left\{ \begin{array}{ccc} j_\alpha & j_p & J \\ j_\beta & j_q & J' \end{array} \right\} V_{p\beta\alpha q J'}^{[12]}, \quad (21)$$

yields a particle-hole contribution only in the [13] channel, whereas the exchange diagram (g), which reads

$$V_{ph} = V_{p\beta q \alpha J}^{[14]} = \sum_{J'} (-)^{2j_q + j_\alpha + j_p + J} \hat{J}'^2 \left\{ \begin{array}{ccc} j_\alpha & j_p & J \\ j_\beta & j_q & J' \end{array} \right\} V_{p\beta q \alpha J'}^{[12]}, \quad (22)$$

results in the corresponding particle-hole contribution in the [14] channel. In electron gas theory, the latter expression is often identified as the starting point for the self-screening of the exchange term. In the discussion of the TDA series in section 4 we will give the expressions for the screening corrections based on Eqs. (21) and (22).

An important aspect to notice in connection with the latter equations and the discussions in sections 4 and 5 is that

$$V_{p\beta q \alpha J}^{[14]} = -V_{p\beta \alpha q J}^{[13]}, \quad (23)$$

i.e., just the exchange diagram, as it should be. This is however important to keep in mind, since we later on will sum explicitly sets of diagrams in the [13] channel and the [14] channel, implying thereby that we will obtain screening and vertex corrections for both direct and exchange diagrams.

### 3 Summation of diagrams in the [12] channel

In order to write down the equation for the renormalized interaction  $\Gamma^{[12]}$  in the [12] channel we need first to present some further definitions. We will also assume that the reader has some familiarity with the theory of Green's function. Thorough discussions of such topics can be found in the recent reviews of Dickoff and Müther [35] and Kuo and Tzeng [36]. In our presentation below we will borrow from these works and the monograph of Blaizot and Ripka [18]. The vertex  $\Gamma^{[12]}$  is in lowest order identical with the interaction  $V^{[12]}$  and obeys also the same symmetry relations as  $V$ , i.e.,

$$\Gamma_{1234J}^{[12]} = \Gamma_{2143J}^{[12]} = -\Gamma_{2134J}^{[12]} = \Gamma_{1243J}^{[12]}. \quad (24)$$

We also need to define energy variables. Since we are going to replace the interaction  $V$  with the  $G$ -matrix, or certain approximations to it, defined below in all of our practical calculations, the momentum variables are already accounted for in  $G$ . The basis will be that of harmonic oscillator wave functions, and the labels 1234 will hence refer to oscillator quantum numbers, which in turn can be related to the momentum variables. The labels 1234, in addition to representing single-particle quantum numbers, define also the energy of the single-particle states. With a harmonic oscillator basis, the starting point for the single-particle energies  $\varepsilon_{1,2,3,4}$  are the unperturbed oscillator energies. When iterating the equations for  $\Gamma^{[12]}$ , self-consistent single-particle energies can be introduced. The total energy in the [12] channel  $s$  is

$$s = \varepsilon_1 + \varepsilon_2 = \varepsilon_3 + \varepsilon_4. \quad (25)$$

The equation for the vertex  $\Gamma^{[12]}$  is, in a compact matrix notation, given by [18]

$$\Gamma^{[12]} = V^{[12]} + V^{[12]}(gg)\Gamma^{[12]}, \quad (26)$$

where  $g$  is the one-body Green's function representing the intermediate states. The diagrammatic expression for this equation is given in Fig. 3. The expression of Eq. (26) is known as the Feynman-Galitskii equation. This equation is normally solved iteratively. In the first iteration the irreducible vertex  $V^{[12]}$  is then often chosen as the bare  $NN$  interaction. This interaction is then typically assumed to be energy independent and we can drop the  $s$  dependence of  $V^{[12]}$ . Moreover, the single-particle propagators are chosen as the

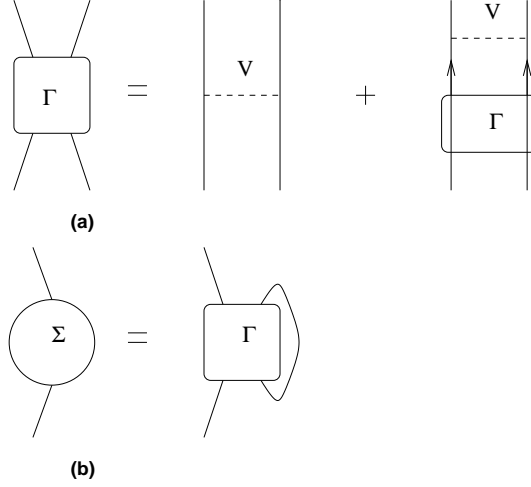


Fig. 3. (a) represents the two-body vertex  $\Gamma$  function while (b) represents the self-energy  $\Sigma$ . unperturbed ones. The first iteration of Eq. (26) can then be rewritten as

$$\Gamma_{1234J}^{[12]}(s) = V_{1234J}^{[12]} + \frac{1}{2} \sum_{56} V_{1256J}^{[12]} \hat{\mathcal{G}}^{[12]} \Gamma_{5634J}^{[12]}(s), \quad (27)$$

with the unperturbed particle-particle and hole-hole propagators

$$\hat{\mathcal{G}}^{[12]} = \frac{Q_{\text{pp}}^{[12]}}{s - \varepsilon_5 - \varepsilon_6 + i\eta} - \frac{Q_{\text{hh}}^{[12]}}{s - \varepsilon_5 - \varepsilon_6 - i\eta}, \quad (28)$$

which results from the integration over the energy variable in the product of the two single-particle propagators in Eq. (26). The factor 1/2 follows from one of the standard Goldstone-Feynman diagram rules [34], which state that a factor 1/2 should be associated with each pair of lines which starts at the same interaction vertex and ends at the same interaction vertex. The reader should note that the intermediate states 56 can represent a two-particle state or a two-hole state. In Eq. (28) we have assumed unperturbed single-particle energies. In our iterations we will approximate the single-particle energies with their real part only. Thus, the two-particle propagator  $\hat{\mathcal{G}}^{[12]}$  with renormalized single-particle energies has the same form as the unperturbed one. The operators  $Q_{\text{pp}}^{[12]}$  and  $Q_{\text{hh}}^{[12]}$  ensure that the intermediate states are of two-particle or two-hole character. In order to obtain a self-consistent scheme, Eq. (27) has also to be accompanied with the equation for the single-particle propagators  $g$  given by Dyson's equation

$$g = g_0 - g_0 \Sigma g, \quad (29)$$

with  $g_0$  being the unperturbed single-particle propagator and  $\Sigma$  the self-energy. We will however defer a discussion of these quantities to section 5. Here it will suffice to state that the self-energy is related to the vertex  $\Gamma^{[12]}$  as

$$\Sigma \sim g \Gamma. \quad (30)$$

The similarity sign is meant to indicate that, although being formally correct, great care has to be exercised in order not to double-count contributions to the self-energy [17]. The set of equations for the vertex function and the self-energy is shown pictorially in Fig. 3. Assume now that we have performed the first iteration. The question which now arises is whether the obtained vertex  $\Gamma^{[12]}$  from the solution of Eq. (27) should replace the bare vertex  $V^{[12]}$  in the next iteration. Before answering this question, let us give some examples of diagrams which can be generated from the first iteration. These contributions are given

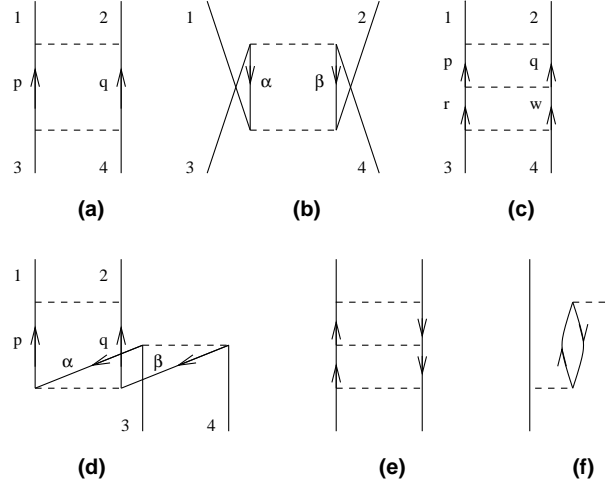


Fig. 4. Diagrams (a)-(d) give examples of diagrams which are summed up by the use of Eq. (26). Diagrams (e) and (f) are examples of core-polarization terms which are not generated by the [12] channel.

by e.g., diagrams (a)-(d) in Fig. 4. Diagrams (a) and (b) are examples of contributions to second order in perturbation theory, while diagrams (c) and (d) are higher order terms. Diagrams (e) and (f) are higher-order core-polarization terms, which can e.g., be generated through the solution of the equations for the [13] and [14] channels discussed in the next section. If we were to include diagrams (a)-(d) in the definition of the bare vertex in our next iteration, we are prone to double-count, since such contributions are generated once again. Diagrams which contain particle-hole intermediate state are however not generated by the solution of Eq. (27). We need therefore to define the vertex  $V^{[12]}$  used in every iteration to be the sum of diagrams which are irreducible in the [12] channel. With irreducible we will mean all diagrams which cannot be reduced to a piece containing the particle states 12 entering or leaving the same interaction vertex and another part containing the states 34 at the same interaction vertex by cutting two internal lines. Clearly, if we cut diagrams (a) and (b) we are just left with two bare interaction vertices. Similarly, cutting two lines of an intermediate state in diagrams (c) and (d) leaves us with two second-order terms of the type (a) and (b) and one bare interaction. Diagrams (e) and (f) are however examples of diagrams which are irreducible in the [12] channel. Diagram (e) is irreducible in the [13] channel, but not in the [14] channel. Similarly, diagram (g) is reducible in the [13] channel and irreducible in the [14] channel. This means that, unless we solve equations similar to

Eq. (27) in the [13] channel and [14] channels as well, changes from further iterations of Eq. (27) will only come from the single-particle terms defined by Dyson's equation in Eq. (29).

In the remaining part of this section, we will try to delineate ways of solving the above equations, and discuss possible approximations, their merits and faults. First of all, we will reduce the propagator of Eq. (28) to only include particle-particle intermediate states. This will lead us to the familiar  $G$ -matrix in nuclear many-body theory. Based on the  $G$ -matrix, we will construct effective interactions through perturbative summations. Applications of such effective interactions to selected nuclei will then be discussed. Thereafter, we will try to account for hole-hole contributions and end this section with a discussion on self-consistent determinations of the single-particle energies through the solution of Dyson's equation.

### 3.1 The $G$ -matrix

In nuclear structure and nuclear matter calculations one has to face the problem that any realistic  $NN$  interaction  $V$  exhibits a strong short-range repulsion, which in turn makes a perturbative treatment of the nuclear many-body problem prohibitive. If the interaction has a so-called hard core, the matrix elements of such an interaction  $\langle \psi | V | \psi \rangle$  evaluated for an uncorrelated two-body wave function  $\psi(r)$  diverge, since the uncorrelated wave function is different from zero also for relative distances  $r$  smaller than the hard-core radius. Similarly, even if one uses interactions with softer cores, the matrix elements of the interaction become very large at short distances. The above problem was however overcome by introducing the reaction matrix  $G^{[12]}$  (displayed by the summation of ladder type of diagrams in Fig. 4 with particle-particle intermediate states only), accounting thereby for short-range two-nucleon correlations. The  $G^{[12]}$ -matrix represents just a subset to the solution of the equations for the interaction  $\Gamma^{[12]}$  in the [12] channel, we have clearly neglected the possibility of having intermediate states which are of the hole-hole type. The matrix elements of the interaction  $V^{[12]}$  then become

$$\langle \psi | G^{[12]} | \psi \rangle = \langle \psi | V^{[12]} | \Psi \rangle \quad (31)$$

where  $\Psi$  is now the correlated wave function containing selected correlation from the excluded space. By accounting for these correlations in the two-body wave function  $\Psi$ , the matrix elements of the interaction become finite, even for a hard-core interaction  $V$ . Moreover, as will be discussed below, compared with the uncorrelated wave function, the correlated wave function enhances the matrix elements of  $V$  at distances for which the interaction is attractive. The type of correlations which typically are included in the evaluation of the  $G^{[12]}$ -matrix are those of the two-particle type. If we label the operator  $Q$  in this case by

$Q_{\text{pp}}^{[12]}$ , we can write the integral equation for the  $G$ -matrix as

$$G^{[12]}(s) = V^{[12]} + V^{[12]} \frac{Q_{\text{pp}}^{[12]}}{s - H_0 + i\eta} G^{[12]}(s), \quad (32)$$

implicitly assuming that  $\lim \eta \rightarrow \infty$ . The variable  $s$  represents normally the unperturbed energy of the incoming two-particle state. We will suppress  $i\eta$  in the following equations. Moreover, since one is often interested only in the  $G^{[12]}$ -matrix for negative starting energies, the  $G^{[12]}$ -matrix commonly used in studies of effective interactions has no divergencies.

We can also write

$$G^{[12]}(s) = V^{[12]} + V^{[12]} Q_{\text{pp}}^{[12]} \frac{1}{s - Q_{\text{pp}}^{[12]} H_0 Q_{\text{pp}}^{[12]}} Q_{\text{pp}}^{[12]} G^{[12]}(s). \quad (33)$$

The former equation applies if the Pauli operator  $Q_{\text{pp}}^{[12]}$  commutes with the unperturbed hamiltonian  $H_0$ , whereas the latter is needed if  $[H_0, Q_{\text{pp}}^{[12]}] \neq 0$ . Similarly, the correlated wave function  $\Psi$  is given as

$$|\Psi\rangle = |\psi\rangle + \frac{Q_{\text{pp}}^{[12]}}{s - H_0} G^{[12]} |\psi\rangle, \quad (34)$$

or

$$|\Psi\rangle = |\psi\rangle + Q_{\text{pp}}^{[12]} \frac{1}{s - Q_{\text{pp}}^{[12]} H_0 Q_{\text{pp}}^{[12]}} Q_{\text{pp}}^{[12]} G^{[12]} |\psi\rangle. \quad (35)$$

In order to evaluate the  $G^{[12]}$ -matrix for finite nuclei, we define first a useful identity following Bethe, Brandow and Petschek [37]. Suppose we have two different  $G$ -matrices<sup>3</sup>, defined by

$$G_1 = V_1 + V_1 \frac{Q_1}{e_1} G_1, \quad (36)$$

and

$$G_2 = V_2 + V_2 \frac{Q_2}{e_2} G_2, \quad (37)$$

where  $Q_1/e_1$  and  $Q_2/e_2$  are the propagators of either Eq. (32) or Eq. (33).  $G_1$  and  $G_2$  are two different  $G$ -matrices having two different interactions and/or different propagators.

---

<sup>3</sup> For notational economy, we drop the superscript <sup>[12]</sup>. Furthermore, in the subsequent discussion in this subsection it is understood that all operators  $Q$  refer to particle-particle intermediate states only. The subscript pp is also dropped.

We aim at an identity which will enable us to calculate  $G_1$  in terms of  $G_2$ , or vice versa. Defining the wave operators

$$\Omega_1 = 1 + \frac{Q_1}{e_1}G_1, \quad (38)$$

and

$$\Omega_2 = 1 + \frac{Q_2}{e_2}G_2, \quad (39)$$

we can rewrite the above  $G$ -matrices as

$$G_1 = V_1\Omega_1, \quad (40)$$

and

$$G_2 = V_2\Omega_2. \quad (41)$$

Using these relations, we rewrite  $G_1$  as

$$\begin{aligned} G_1 &= G_1 - G_2^\dagger \left( \Omega_1 - 1 - \frac{Q_1}{e_1}G_1 \right) + \left( \Omega_2^\dagger - 1 - G_2^\dagger \frac{Q_2}{e_2} \right) G_1 \\ &= G_2^\dagger + G_2^\dagger \left( \frac{Q_1}{e_1} - \frac{Q_2}{e_2} \right) G_1 + \Omega_2^\dagger G_1 - G_2^\dagger \Omega_1, \end{aligned} \quad (42)$$

and using Eqs. (40) and (41) we obtain the identity

$$G_1 = G_2^\dagger + G_2^\dagger \left( \frac{Q_1}{e_1} - \frac{Q_2}{e_2} \right) G_1 + \Omega_2^\dagger (V_1 - V_2) \Omega_1. \quad (43)$$

The second term on the rhs. is called the propagator-correction term; it vanishes if  $G_1$  and  $G_2$  have the same propagators. The third term is often referred to as the potential-correction term, and it disappears if  $G_1$  and  $G_2$  have the same potentials. The reader may now ask what is the advantage of the above identity. If we assume that by some physical reasoning we are able to calculate  $G_2$  and that the expression for  $G_2$  can be calculated easily, and further that  $G_2$  is a good approximation to the original  $G$ -matrix, then we can use the above identity to perform a perturbative calculation of  $G_1$  in terms of  $G_2$ .

Before we proceed in detailing the calculation of the  $G$ -matrix appropriate for finite nuclei, certain approximations need be explained.

As discussed above, the philosophy behind perturbation theory is to reduce the intractable full Hilbert space problem to one which can be solved within a physically motivated model space, defined by the operator  $P$ . The excluded degrees of freedom are represented by the projection operator  $Q$ . The definition of these operators is connected with the nuclear

|       |                |              |
|-------|----------------|--------------|
| ⋮     |                | Orbit number |
| _____ | 4s-3d-2g-1i-0k | 37-45        |
| _____ | 3p-2f-1h-0j    | 29-36        |
| _____ | 3s-2d-1g-0i    | 22-28        |
| _____ | 2p-1f-0h       | 16-21        |
| _____ | 2s-1d-0g       | 11-15        |
| _____ | 1p-0f          | 7-10         |
| _____ | 1s-0d          | 4-6          |
| _____ | 0p             | 2-3          |
| _____ | 0s             | 1            |

Fig. 5. Classification of harmonic oscillator single-particle orbits.

system and the perturbative expansions discussed in section 2. Consider the evaluation of the effective interaction needed in calculations of the low-lying states of  $^{18}\text{O}$ . From experimental data and theoretical calculations the belief is that several properties of this nucleus can be described by a model space consisting of a closed  $^{16}\text{O}$  core (consisting of the filled  $0s$ - and  $0p$ -shells) and two valence neutrons in the  $1s0d$ -shell. In Fig. 5 we exhibit this division in terms of h.o. sp orbits. The active sp states in the  $1s0d$ -shell are then given by the  $0d_{5/2}$ ,  $0d_{3/2}$  and  $1s_{1/2}$  orbits, labels 4 – 6 in Fig. 5. The remaining states enter the definition of  $Q$ . Once we have defined  $P$  and  $Q$  we proceed in constructing the  $G$ -matrix and the corresponding perturbative expansion in terms of the  $G$ -matrix. There are however several ways of choosing  $Q$ . A common procedure is to specify the boundaries of  $Q$  by three numbers,  $n_1$ ,  $n_2$  and  $n_3$ , explained in Fig. 6. For  $^{18}\text{O}$  we would choose

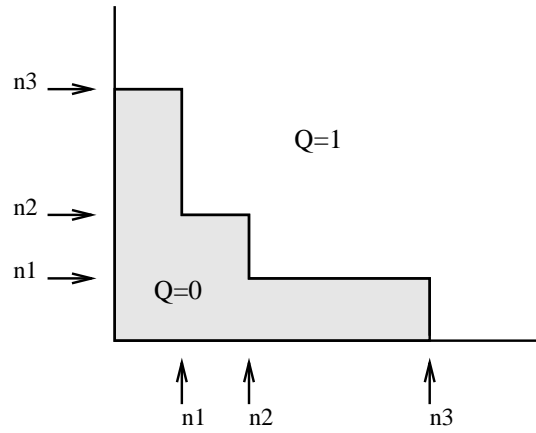


Fig. 6. Definition of the  $P$  (shaded area) and  $Q$  operators appropriate for the definition of the  $G$ -matrix and the effective interaction. Outside the shaded area limited by the boundaries  $n_1$ ,  $n_2$  and  $n_3$   $P = 0$  and  $Q = 1$ .

( $n_1 = 3, n_2 = 6, n_3 = \infty$ ). Our choice of  $P$ -space implies that the single-particle states

outside the model space start from the  $1p0f$ -shell (numbers 7–10 in Fig. 5), and orbits 1, 2 and 3 are hole states. Stated differently, this means that  $Q$  is constructed so as to prevent scattering into intermediate two-particle states with one particle in the  $0s$ - or  $0p$ -shells or both particles in the  $1s0d$ -shell. This definition of the  $Q$ -space influences the determination of the effective shell-model interaction. Consider the diagrams displayed in Fig. 7. Diagram (a) of this figure is just the  $G$ -matrix and is allowed in the definition of

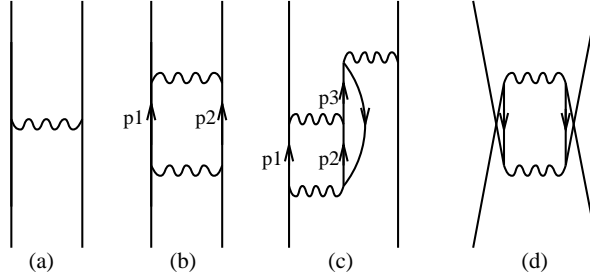


Fig. 7. Examples of diagrams which may define the effective valence space interaction. The wavy line is the  $G$ -matrix.

the  $\hat{Q}$ -box. With our choice ( $n_1 = 3, n_2 = 6, n_3 = \infty$ ), diagram (b) is not allowed since the intermediate state consists of passive particle states and is already included in the evaluation of the  $G$ -matrix. Similarly, diagram (c) is also not allowed whereas diagram (d) is allowed. Now an important subtlety arises. If we evaluate the  $G$ -matrix with the boundaries ( $n_1 = 3, n_2 = 10, n_3 = \infty$ ), and define the  $P$ -space of the *effective interaction* by including orbits 4 to 6 only, then diagrams (b) and (c) are allowed if  $7 \leq p_1, p_2 \leq 10$ . In this way we allow for intermediate two-particle states as well with orbits outside the model-space of the effective interaction. The reader should notice the above differences, i.e. that the  $Q$ -space defining the  $G$ -matrix and  $H_{\text{eff}}$  may differ. In order to calculate the  $G$ -matrix we will henceforth employ a so-called double-partitioned scheme. Let us be more specific and detail this double-partitioned procedure. We define first a reference  $G$ -matrix  $\bar{G}$  in terms of plane wave intermediate states only, meaning that  $H_0$  is replaced by the kinetic energy operator  $T$  only while  $G$  has harmonic oscillator intermediate states (this is one possible choice for  $U$ ). We divide the exclusion operator into two parts, one which represents the low-lying states  $Q_l$  and one which accounts for high-lying states  $Q_h$ , viz.

$$Q = Q_l + Q_h = Q_l + \tilde{Q}.$$

If we consider  $^{18}\text{O}$  as our pilot nucleus, we may define  $Q_l$  to consist of the  $sp$  orbits of the  $1p0f$ -shell, orbits 7 – 10 in Fig. 5, described by h.o. states.  $Q_h$  represents then the remaining orthogonalized intermediate states. Using the identity of Bethe, Brandow and

Petschek [37] of Eq. (43) we can first set up  $\tilde{G}$  as

$$\tilde{G} = V + V \frac{\tilde{Q}}{s - T} \tilde{G}, \quad (44)$$

and express  $G$  in terms of  $\tilde{G}$  as

$$G = \tilde{G} + \tilde{G} \left( \frac{Q_l}{s - H_0} \right) G, \quad (45)$$

and we have assumed that  $\tilde{G}$  is hermitian and that  $[Q_l, H_0] = 0$ . Thus, we first calculate a “reference”  $G$ -matrix ( $\tilde{G}$  in our case), and then insert this in the expression for the full  $G$ -matrix. The novelty here is that we are able to calculate  $\tilde{G}$  exactly through operator relations to be discussed below. In passing we note that  $G$  depends significantly on the choice of  $H_0$ , though the low-lying intermediate states are believed to be fairly well represented by h.o. states. Also, the authors of ref. [38] demonstrate that low-lying intermediate states are not so important in  $G$ -matrix calculations, being consistent with the short-range nature of the  $NN$  interaction. Since we let  $Q_l$  to be defined by the orbits of the  $1p0f$ -shell, and the energy difference between two particles in the  $sd$ -shell and  $pf$  shell is of the order  $-14$  MeV, we can treat  $G$  as a perturbation expansion in  $\tilde{G}$ . Eq. (45) can then be written as

$$G = \tilde{G} + \tilde{G} \left( \frac{Q_l}{s - H_0} \right) \tilde{G} + \tilde{G} \left( \frac{Q_l}{s - H_0} \right) \tilde{G} \left( \frac{Q_l}{s - H_0} \right) \tilde{G} + \dots \quad (46)$$

The only intermediate states are those defined by the  $1p0f$ -shell. The second term on the rhs. is nothing but the second-order particle-particle ladder. The third term is then the third-order ladder diagram in terms of  $\tilde{G}$ . As shown by the authors of ref. [38], the inclusion of the second-order particle-particle diagram in the evaluation of the  $\hat{Q}$ -box, represents a good approximation. The unsettled problem is however how to define the boundary between  $Q_l$  and  $Q_h$ .

Now we will discuss how to compute  $\tilde{G}$ . One can solve the equation for the  $G$ -matrix for finite nuclei by employing a formally exact technique for handling  $\tilde{Q}$  discussed in e.g., Ref. [38]. Using the matrix identity

$$\tilde{Q} \frac{1}{\tilde{Q}A\tilde{Q}} \tilde{Q} = \frac{1}{A} - \frac{1}{A} \tilde{P} \frac{1}{\tilde{P}A^{-1}\tilde{P}} \tilde{P} \frac{1}{A}, \quad (47)$$

with  $A = s - T$ , to rewrite Eq. (44) as<sup>4</sup>

$$G = G_F + \Delta G, \quad (48)$$

---

<sup>4</sup>We will omit the label  $\tilde{G}$  for the  $G$ -matrix for finite nuclei, however it is understood that the  $G$ -matrix for finite nuclei is calculated according to Eq. (44) This means that we have to include the particle-particle ladder diagrams in the  $\hat{Q}$ -box.

where  $G_F$  is the free  $G$ -matrix defined as

$$G_F = V + V \frac{1}{s - T} G_F. \quad (49)$$

The term  $\Delta G$  is a correction term defined entirely within the model space  $\tilde{P}$  and given by

$$\Delta G = -V \frac{1}{A} \tilde{P} \frac{1}{\tilde{P} A^{-1} \tilde{P}} \tilde{P} \frac{1}{A} V. \quad (50)$$

Employing the definition for the free  $G$ -matrix of Eq. (49), one can rewrite the latter equation as

$$\Delta G = -G_F \frac{1}{e} \tilde{P} \frac{1}{\tilde{P}(e^{-1} + e^{-1} G_F e^{-1}) \tilde{P}} \tilde{P} \frac{1}{e} G_F, \quad (51)$$

with  $e = s - T$ . We see then that the  $G$ -matrix for finite nuclei is expressed as the sum of two terms; the first term is the free  $G$ -matrix with no Pauli corrections included, while the second term accounts for medium modifications due to the Pauli principle. The second term can easily be obtained by some simple matrix operations involving the model-space matrix  $\tilde{P}$  only. However, the second term is a function of the variable  $n_3$ . The convergence in terms of  $n_3$  was discussed ad extenso in Ref. [4] and we refer the reader to that work. The equation for the free matrix  $G_F$  is solved in momentum space in the relative and centre of mass system and thereafter transformed to the relevant expression in terms of harmonic oscillator single-particle wavefunctions in the laboratory system. This yields final matrix elements of the type

$$\langle (ab)J | G | (cd)J \rangle \quad (52)$$

where  $G$  is the given by the sum  $G = G_F + \Delta G$ . The label  $a$  represents here all the single particle quantum numbers  $n_a l_a j_a$ .

### 3.2 *Folded diagrams and the effective valence space interaction*

Here we discuss further classes of diagrams which can be included in the evaluation of effective interactions for the shell model. Especially, we will focus on the summations of so-called folded diagrams.

One way of obtaining the wave operator  $\Omega$  is through the generalized Bloch equation given by Lindgren and Morrison [5]

$$[\Omega, H_0]P = QH_1\Omega P - \chi PH_1\Omega P, \quad (53)$$

which offers a suitable way of generating the RS perturbation expansion. Writing Eq. (53) in terms of  $\Omega^{(n)}$  we have

$$[\Omega^{(1)}, H_0]P = QH_1P, \quad (54)$$

$$[\Omega^{(2)}, H_0]P = QH_1\Omega^{(1)}P - \Omega^{(1)}PH_1P, \quad (55)$$

and so forth, which can be generalized to

$$[\Omega^{(n)}, H_0]P = QH_1\Omega^{(n-1)}P - \sum_{m=1}^{n-1} \Omega^{(n-m)}PH_1\Omega^{(m-1)}P. \quad (56)$$

The effective interaction to a given order can then be obtained from  $\Omega^{(n)}$ , see [5]. Another possibility is obviously the coupled-cluster method discussed elsewhere in this volume.

Here we will assume that we can start with a given approximation to  $\Omega$ , and through an iterative scheme generate higher order terms. Such schemes will in general differ from the order-by-order scheme of Eq. (53). Two such iterative schemes were derived by Lee and Suzuki [39]. We will focus on the folded diagram method of Kuo and co-workers [3].

Having defined the wave operator  $\Omega = 1 + \chi$  (note that  $\Omega^{-1} = 1 - \chi$ ) with  $\chi$  given by Eq. (9) we can obtain

$$QHP - \chi HP + QH\chi - \chi H\chi = 0. \quad (57)$$

This is the basic equation to which a solution to  $\chi$  is to be sought. If we choose to work with a degenerate model space we define

$$PH_0P = sP,$$

where  $s$  is the unperturbed model space eigenvalue (or starting energy) in the degenerate case, such that Eq. (57) reads in a slightly modified form ( $H = H_0 + H_1$ )

$$(s - QH_0Q - QH_1Q)\chi = QH_1P - \chi PH_1P - \chi PH_1Q\chi,$$

which yields the following equation for  $\chi$

$$\chi = \frac{1}{s - QHQ}QH_1P - \frac{1}{s - QHQ}\chi(PH_1P + PH_1Q\chi P). \quad (58)$$

Observing that the  $P$ -space effective hamiltonian is given as

$$H_{\text{eff}} = PHP + PH\chi = PH_0P + V_{\text{eff}}(\chi),$$

with  $V_{\text{eff}}(\chi) = PH_1P + PH_1Q\chi P$ , Eq. (58) becomes

$$\chi = \frac{1}{s - QHQ}QH_1P - \frac{1}{s - QHQ}\chi V_{\text{eff}}(\chi). \quad (59)$$

Now we find it convenient to introduce the so-called  $\hat{Q}$ -box, defined as

$$\hat{Q}(s) = PH_1P + PH_1Q \frac{1}{s - QHQ} QH_1P. \quad (60)$$

The  $\hat{Q}$ -box is made up of non-folded diagrams which are irreducible and valence linked. A diagram is said to be irreducible if between each pair of vertices there is at least one hole state or a particle state outside the model space. In a valence-linked diagram the interactions are linked (via fermion lines) to at least one valence line. Note that a valence-linked diagram can be either connected (consisting of a single piece) or disconnected. In the final expansion including folded diagrams as well, the disconnected diagrams are found to cancel out [3]. This corresponds to the cancellation of unlinked diagrams of the Goldstone expansion. We illustrate these definitions by the diagrams shown in Fig. 8. Diagram (a)

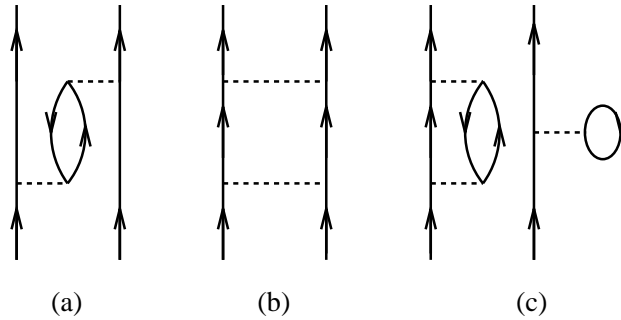


Fig. 8. Different types of valence-linked diagrams. Diagram (a) is irreducible and connected, (b) is reducible, while (c) is irreducible and disconnected.

is irreducible, valence linked and connected, while (b) is reducible since the intermediate particle states belong to the model space. Diagram (c) is irreducible, valence linked and disconnected. It is worth noting that general form of the  $\hat{Q}$ -box is the same as that of the  $G$ -matrix, or the equations of the [12] channel or those of the [13] and [14] channels to be discussed in section 4. In Ref. [4], the  $\hat{Q}$ -box was defined to be the sum all diagrams to third order in the  $G$ -matrix.

Multiplying both sides of Eq. (59) with  $PH_1$  and adding  $PH_1P$  to both sides we get

$$PH_1P + PH_1\chi = PH_1P + PH_1Q \frac{1}{s - QHQ} QH_1P - PH_1 \frac{1}{s - QHQ} \chi V_{\text{eff}}(\chi),$$

which gives

$$V_{\text{eff}}(\chi) = \hat{Q}(s) - PH_1 \frac{1}{s - QHQ} \chi V_{\text{eff}}(\chi). \quad (61)$$

There are several ways to solve Eq. (61). The idea is to set up an iteration scheme where we determine  $\chi_n$  and thus  $V_{\text{eff}}(\chi_n)$  from  $\chi_{n-1}$  and  $V_{\text{eff}}(\chi_{n-1})$ . For the mere sake of simplicity we write  $V_{\text{eff}}^{(n)} = V_{\text{eff}}(\chi_n)$ .

Let us write Eq. (61) as

$$V_{\text{eff}}^{(n)} = \hat{Q}(s) - PH_1 \frac{1}{s - QHQ} \chi_n V_{\text{eff}}^{(n-1)}.$$

The solution to this equation can be shown to be [39]

$$V_{\text{eff}}^{(n)} = \hat{Q} + \sum_{m=1}^{\infty} \frac{1}{m!} \frac{d^m \hat{Q}}{ds^m} \left\{ V_{\text{eff}}^{(n-1)} \right\}^m. \quad (62)$$

Observe also that the effective interaction is  $V_{\text{eff}}^{(n)}$  is evaluated at a given model space energy  $s$ . If  $V_{\text{eff}}^{(n)} = V_{\text{eff}}^{(n-1)}$ , the iteration is said to converge. In the limiting case  $n \rightarrow \infty$ , the solution  $V_{\text{eff}}^{(\infty)}$  agrees with the formal solution of Brandow [2] and Des Cloizeaux [40]

$$V_{\text{eff}}^{(\infty)} = \sum_{m=0}^{\infty} \frac{1}{m!} \frac{d^m \hat{Q}}{ds^m} \left\{ V_{\text{eff}}^{(\infty)} \right\}^m. \quad (63)$$

Alternatively, we can generate the contribution from  $n$  folds the following way. In an  $n$ -folded  $\hat{Q}$ -box there are of course  $n + 1$   $\hat{Q}$ -boxes. The general expression for an  $n$ -folded  $\hat{Q}$ -box is then

$$\hat{Q} - \hat{Q} \int \hat{Q} + \hat{Q} \int \hat{Q} \int \hat{Q} - \dots = \sum_{m_1 m_2 \dots m_n} \frac{1}{m_1!} \frac{d^{m_1} \hat{Q}}{ds^{m_1}} P \frac{1}{m_2!} \frac{d^{m_2} \hat{Q}}{ds^{m_2}} P \dots \frac{1}{m_n!} \frac{d^{m_n} \hat{Q}}{ds^{m_n}} P \hat{Q}, \quad (64)$$

where we have the constraints

$$m_1 + m_2 + \dots m_n = n,$$

$$m_1 \geq 1,$$

$$m_2, m_3, \dots m_n \geq 0,$$

and

$$m_k \leq n - k + 1.$$

The last restriction follows from the fact that there are only  $n - k + 1$   $\hat{Q}$ -boxes to the right of  $k^{\text{th}}$   $\hat{Q}$ -box. Thus, it can at most be differentiated  $n - k + 1$  times. We have inserted the model-space projection operator in the above expression, in order to emphasize that folded diagrams have as intermediate states between successive  $\hat{Q}$ -boxes only model-space states. Therefore, the sum in Eq. (64) includes a sum over all model-space states with the same quantum numbers such as isospin and total angular momentum. It is understood that the  $\hat{Q}$ -box and its derivatives are evaluated at the same starting energy, which should correspond to the unperturbed energy of the model-space state. It is then straightforward to recast Eq. (64) into the form of Eq. (62).

Note that although  $\hat{Q}$  and its derivatives contain disconnected diagrams, such diagrams cancel exactly in each order [3], thus yielding a fully connected expansion in Eq. (62). However, in order to achieve this, disconnected diagrams have to be included in the definition of the  $\hat{Q}$ -box. An example is given by diagram (c) Fig. 8. Such a diagram will generate a contribution to the first fold  $\frac{d\hat{Q}}{ds}\hat{Q} = -\hat{Q} \int \hat{Q}$  which cancels exactly diagram (c) when all time-ordered contributions to this diagram are accounted for, see Ref. [3] for more details. It is moreover important to note in connection with the above expansion, that a term like  $F_1 = \hat{Q}_1\hat{Q}$  actually means  $P\hat{Q}_1P\hat{Q}P$  since the  $\hat{Q}$ -box is defined in the model space only. Here we have defined  $\hat{Q}_m = \frac{1}{m!} \frac{d^m \hat{Q}}{ds^m}$ . Due to this structure, only so-called folded diagrams contain  $P$ -space intermediate states.

The folded diagram expansion discussed above yields however a non-hermitian effective interaction. This may happen even at the level of the  $G$ -matrix, or any of the effective interactions we will derive in this work, from Parquet theory to the order-by-order perturbation expansion.

We will therefore end this section with a way to cure this non-hermiticity. A hermitian effective interaction has recently been derived by Ellis, Kuo, Suzuki and co-workers [1,6,41] through the following steps<sup>5</sup>. To obtain a hermitian effective interaction, let us define a model-space eigenstate  $|b_\lambda\rangle$  with eigenvalue  $\lambda$  as

$$|b_\lambda\rangle = \sum_{\alpha=1}^D b_\alpha^{(\lambda)} |\psi_\alpha\rangle \quad (65)$$

and the biorthogonal wave function

$$|\bar{b}_\lambda\rangle = \sum_{\alpha=1}^D \bar{b}_\alpha^{(\lambda)} |\bar{\psi}_\alpha\rangle, \quad (66)$$

such that

$$\langle \bar{b}_\lambda | b_\mu \rangle = \delta_{\lambda\mu}. \quad (67)$$

The model-space eigenvalue problem can be written in terms of the above non-hermitian effective interaction unperturbed wave functions

$$\sum_{\gamma=1}^D b_\gamma^{(\lambda)} \langle \psi_\sigma | H_0 + V + VQ\chi | \psi_\gamma \rangle = E_\lambda b_\sigma^{(\lambda)}. \quad (68)$$

The exact wave function expressed in terms of the correlation operator is

$$|\Psi_\lambda\rangle = (\mathbf{1} + \chi) |\psi_\lambda\rangle. \quad (69)$$

---

<sup>5</sup> The reader who wishes more details can consult Refs. [1,41].

The part  $\chi|\psi_\lambda\rangle$  can be expressed in terms of the time-development operator or using the time-independent formalism as

$$\chi|\psi_\lambda\rangle = \frac{Q}{E_\lambda - QHQ}QVP|\psi_\lambda\rangle, \quad (70)$$

where  $Q$  is the exclusion operator. Note that this equation is given in terms of the Brillouin-Wigner perturbation expansion, since we have the exact energy  $E_\lambda$  in the denominator.

Using the normalization condition for the true wave function we obtain

$$\langle\Psi_\gamma|\Psi_\lambda\rangle N_\lambda\delta_{\lambda\gamma} = \langle\psi_\gamma|(\mathbf{1} + \chi^\dagger\chi)|\psi_\lambda\rangle, \quad (71)$$

where we have used the fact that  $\langle\psi_\gamma|\chi|\psi_\lambda\rangle = 0$ . Recalling that the time-development operator is hermitian we have that  $\chi^\dagger\chi$  is also hermitian. We can then define an orthogonal basis  $d$  whose eigenvalue relation is

$$\sum_\alpha \langle\psi_\beta|\chi^\dagger\chi|\psi_\alpha\rangle d_\alpha^\lambda = \mu_\lambda^2 d_\beta^\lambda, \quad (72)$$

with eigenvalues greater than 0. Using the definition in Eq. (70), we note that the diagonal element of

$$\langle\psi_\lambda|\chi^\dagger\chi|\psi_\lambda\rangle = \langle\psi_\lambda|PVQ\frac{1}{(E_\lambda - QHQ)^2}QVP|\psi_\lambda\rangle, \quad (73)$$

which is nothing but the derivative of the  $\hat{Q}$ -box, with an additional minus sign. Thus, noting that if  $\gamma \neq \lambda$

$$\langle\Psi_\gamma|\Psi_\lambda\rangle = 0 = \langle\psi_\gamma|\psi_\lambda\rangle + \langle\psi_\gamma|\chi^\dagger\chi|\psi_\lambda\rangle, \quad (74)$$

we can write  $\chi^\dagger\chi$  in operator form as

$$\chi^\dagger\chi = -\sum_\alpha |\bar{\psi}_\alpha\rangle \langle\psi_\alpha| \hat{Q}_1(E_\alpha) |\psi_\alpha\rangle \langle\bar{\psi}_\alpha| - \sum_{\alpha \neq \beta} |\bar{\psi}_\alpha\rangle \langle\psi_\alpha|\psi_\beta\rangle |\bar{\psi}_\beta\rangle. \quad (75)$$

Using the new basis in Eq. (72), we see that Eq. (71) allows us to define another orthogonal basis  $h$

$$h_\alpha^\lambda = \sqrt{\mu_\alpha^2 + 1} \sum_\beta d_\beta^\alpha b_\beta^\lambda \frac{1}{\sqrt{N_\lambda}} = \frac{1}{\sqrt{\mu_\alpha^2 + 1}} \sum_\beta d_\beta^\alpha \bar{b}_\beta^\lambda \sqrt{N_\lambda}, \quad (76)$$

where we have used the orthogonality properties of the vectors involved. The vector  $h$  was used by the authors of Ref. [41] to obtain a hermitian effective interaction as

$$\langle\psi_\alpha|V_{\text{eff}}^{(\text{her})}|\psi_\beta\rangle = \frac{\sqrt{\mu_\alpha^2 + 1} \langle\psi_\alpha|V_{\text{eff}}^{(\text{nher})}|\psi_\beta\rangle + \sqrt{\mu_\beta^2 + 1} \langle\psi_\alpha|V_{\text{eff}}^{\dagger(\text{nher})}|\psi_\beta\rangle}{\sqrt{\mu_\alpha^2 + 1} + \sqrt{\mu_\beta^2 + 1}}, \quad (77)$$

where (her) and (nher) stand for hermitian and non-hermitian respectively. This equation is rather simple to compute, since we can use the folded-diagram method to obtain the non-hermitian part. To obtain the total hermitian effective interaction, we have to add the  $H_0$  term. The above equation is manifestly hermitian. Other discussion of the hermiticity problem can be found in Refs. [5,7]. The remaining question is how to evaluate the  $\hat{Q}$ -box. Obviously, we are not in the position where we can evaluate it exactly, i.e., to include all possible many-body terms. Rather, we have to truncate somewhere. Several possible approaches exist, but all have in common that there is no clear way which tells us where to stop. However, as argued by the authors of Ref. [17], there is a minimal class of diagrams which need to be included in order to fulfill necessary conditions. This class of diagrams includes both diagrams which account for short-range correlations such as the  $G$ -matrix and long-range correlations such as those accounted for by various core-polarization terms. The importance of such diagrams has been extensively documented in the literature and examples can be found in Refs. [4,26]. In Ref. [4] we included all core-polarization contributions to third-order in the  $G$ -matrix, in addition to including other diagrams which account for short-range correlations as well.

In the next subsection we present results from recent large scale shell-model Monte Carlo calculations [42] for light nuclei in the  $1s0d$  and  $1p0f$  shells based on an effective interaction for the two shells. The effective interaction was derived following the methods outlined hitherto in this section, taking into account the non-hermiticity which arises when dealing with more than one major shell. The closed shell core is  $^{16}\text{O}$  and all diagrams through second-order were employed in the definition of the  $\hat{Q}$ -box. Folded diagrams were calculated using the abovementioned folded-diagrams method and the interaction was made explicitly hermitian through Eq. (77). A discussion of results for Sn isotopes will also be given.

### 3.3 Selected applications

#### 3.3.1 Neutron-rich nuclei in the $1s0d$ - $1p0f$ shells

Studies of extremely neutron-rich nuclei have revealed a number of intriguing new phenomena. Two sets of these nuclei that have received particular attention are those with neutron number  $N$  in the vicinity of the  $1s0d$  and  $0f_{7/2}$  shell closures ( $N \approx 20$  and  $N \approx 28$ ). Experimental studies of neutron-rich Mg and Na isotopes indicate the onset of deformation, as well as the modification of the  $N = 20$  shell gap for  $^{32}\text{Mg}$  and nearby nuclei [43]. Inspired by the rich set of phenomena occurring near the  $N = 20$  shell closure when  $N \gg Z$ , attention has been directed to nuclei near the  $N = 28$  (sub)shell closure for a number of S and Ar isotopes [44,45] where similar, but less dramatic, effects have been seen as well. In parallel with the experimental efforts, there have been several theoretical studies seeking to understand and, in some cases, predict properties of these unstable nuclei. Both mean-field

Table 1

The computed and measured values of  $B(E2)$  for the nuclei in this study using  $e_p = 1.5$  and  $e_n = 0.5$ .

|                  | $B(E2; 0_{gs}^+ \rightarrow 2_1^+)_{Expt}$ | $B(E2, total)_{SMMC}$ | $B(E2; 0_{gs}^+ \rightarrow 2_1^+)$ |
|------------------|--|-----------------------|-------------------------------------|
| $^{22}\text{Mg}$ | $458 \pm 183$                              | $334 \pm 27$          |                                     |
| $^{30}\text{Ne}$ |  | $303 \pm 32$          | 342 [50], 171 [59]                  |
| $^{32}\text{Mg}$ | $454 \pm 78$ [43]                          | $494 \pm 44$          | 448 [50], 205 [59]                  |
| $^{36}\text{Ar}$ | $296.56 \pm 28.3$ [57]                     | $174 \pm 48$          |                                     |
| $^{40}\text{S}$  | $334 \pm 36$ [44]                          | $270 \pm 66$          | 398 [45], 390 [51]                  |
| $^{42}\text{S}$  | $397 \pm 63$ [44]                          | $194 \pm 64$          | 372 [45], 465 [51]                  |
| $^{42}\text{Si}$ |  | $445 \pm 62$          | 260 [51]                            |
| $^{44}\text{S}$  | $314 \pm 88$ [45]                          | $274 \pm 68$          | 271 [45], 390 [51]                  |
| $^{44}\text{Ti}$ | $610 \pm 150$ [58]                         | $692 \pm 63$          |                                     |
| $^{46}\text{Ar}$ | $196 \pm 39$ [44]                          | $369 \pm 77$          | 460 [44], 455 [51]                  |

[46,47] and shell-model calculations [44,45,48–52] have been proposed. The latter require a severe truncation to achieve tractable model spaces, since the successful description of these nuclei involves active nucleons in both the  $1s0d$ - and the  $1p0f$ -shells. The natural basis for the problem is therefore the full  $1s0d$ - $1p0f$  space, which puts it out of reach of exact diagonalization on current hardware<sup>6</sup>.

Shell-Model Monte Carlo (SMMC) methods [?,53,54] offer an alternative to direct diagonalization when the bases become very large. Though SMMC provides limited detailed spectroscopic information, it can predict, with good accuracy, overall nuclear properties such as masses, total strengths, strength distributions, and deformation, precisely those quantities probed by the recent experiments.

There is limited experimental information about the highly unstable, neutron-rich nuclei under consideration. In many cases only the mass, excitation energy of the first excited state, the  $B(E2)$  to that state, and the  $\beta$ -decay rate is known, and not even all of this information is available in some cases. From the measured  $B(E2)$ , an estimate of the nuclear deformation parameter,  $\beta_2$ , has been obtained via the usual relation

$$\beta_2 = 4\pi \sqrt{B(E2; 0_{gs}^+ \rightarrow 2_1^+) / 3ZR_0^2 e} \quad (78)$$

with  $R_0 = 1.2A^{1/3}$  fm and  $B(E2)$  given in  $e^2\text{fm}^4$ .

Much of the interest in the region stems from the unexpectedly large values of the deduced

<sup>6</sup> For a treatment of the c.m. problem, see Ref. [42].

$\beta_2$ , results which suggest the onset of deformation and have led to speculations about the vanishing of the  $N = 20$  and  $N = 28$  shell gaps. The lowering in energy of the  $2_1^+$  state supports this interpretation. The most thoroughly studied case, and the one which most convincingly demonstrates these phenomena, is  $^{32}\text{Mg}$  with its extremely large  $B(E2) = 454 \pm 78 e^2\text{fm}^4$  and corresponding  $\beta_2 = 0.513$  [43]; however, a word of caution is necessary when deciding on the basis of this limited information that we are in the presence of well-deformed rotors: for  $^{22}\text{Mg}$ , we would obtain  $\beta_2 = 0.67$ , even more spectacular, and for  $^{12}\text{C}$ ,  $\beta_2 = 0.8$ , well above the superdeformed bands.

Most of the measured observables can be calculated within the SMMC framework. It is well known that in *deformed* nuclei the total  $B(E2)$  strength is almost saturated by the  $0_{gs}^+ \rightarrow 2_1^+$  transition (typically 80% to 90% of the strength lies in this transition). Thus the total strength calculated by SMMC should only slightly overestimate the strength of the measured transition. In Table 1 the SMMC computed values of  $B(E2, \text{total})$  are compared both to the experimental  $B(E2; 0_{gs}^+ \rightarrow 2_1^+)$  values and to the values found in various truncated shell-model calculations. Reasonable agreement with experimental data across the space is obtained when one chooses effective charges of  $e_p = 1.5$  and  $e_n = 0.5$ . All of the theoretical calculations require excitations to the  $1p0f$ -shell before reasonable values can be obtained. We note a general agreement among all calculations of the  $B(E2)$  for  $^{46}\text{Ar}$ , although they are typically larger than experimental data would suggest. We also note a somewhat lower value of the  $B(E2)$  in this calculation as compared to experiment and other theoretical calculations in the case of  $^{42}\text{S}$ . Table 2 gives selected occupation numbers for the nuclei considered. We first note a difficulty in extrapolating some of the occupations where the number of particles is nearly zero. This leads to a systematic error bar that we estimate at  $\pm 0.2$  for all occupations shown, while the statistical error bar is quoted in the table. The extrapolations for occupation numbers were principally linear. Table 2 shows that  $^{22}\text{Mg}$  remains as an almost pure *sd*-shell nucleus, as expected. We also see that the protons in  $^{30}\text{Ne}$ ,  $^{32}\text{Mg}$ , and  $^{42}\text{Si}$  are almost entirely confined to the *sd* shell. This latter is a pleasing result in at least two regards. First, it shows that the interaction does not mix the two shells to an unrealistically large extent. Second, if spurious c.m. contamination were a severe problem, we would expect to see a larger proton  $0f_{7/2}$  population for these nuclei due to the  $0d_{5/2} \rightarrow 0f_{7/2}$  “transition” mediated by the center-of-mass creation operator. The fact that there is little proton  $f_{7/2}$  occupation for these nuclei confirms that the c.m. contamination is under reasonable control. See Ref. [42] for further details. An interesting feature of Table 2 lies in the neutron occupations of the  $N = 20$  nuclei ( $^{30}\text{Ne}$  and  $^{32}\text{Mg}$ ) and the  $N = 28$  nuclei ( $^{42}\text{Si}$ ,  $^{44}\text{S}$ , and  $^{46}\text{Ar}$ ). The neutron occupations of the two  $N = 20$  nuclei are quite similar, confirming the finding of Fukunishi *et al.* [50] and Poves and Retamosa [49] that the  $N = 20$  shell gap is modified. In fact, the neutron  $0f_{7/2}$  orbital contains approximately two particles before the  $N = 20$  closure, thus behaving like an intruder single-particle state. Furthermore, we see that 2p-2h excitations dominate although higher excitations also play some role. We also see that the neutrons occupying the  $1p0f$ -shell in  $N = 20$  systems are principally confined to the  $0f_{7/2}$  sub-shell. The conclusions that follow from looking at nuclei with  $N > 20$ , particularly those with  $N = 28$ , are that the

Table 2

The calculated SMMC neutron and proton occupation numbers for the  $sd$  shell, the  $0f_{7/2}$  sub-shell, and the remaining orbitals of the  $pf$  shell. The statistical errors are given for linear extrapolations. A systematic error of  $\pm 0.2$  should also be included. The first row represents neutron results, while the second row represents protons.

|                  | $N, Z$ | $1s0d$           | $0f_{7/2}$       | $1p0f_{5/2}$     |
|------------------|--------|------------------|------------------|------------------|
| $^{22}\text{Mg}$ | 10,12  | $3.93 \pm 0.02$  | $0.1 \pm 0.02$   | $-0.05 \pm 0.01$ |
|                  |        | $2.04 \pm 0.02$  | $0.00 \pm 0.01$  | $-0.05 \pm 0.01$ |
| $^{30}\text{Ne}$ | 20,10  | $9.95 \pm 0.03$  | $2.32 \pm 0.03$  | $-0.26 \pm 0.02$ |
|                  |        | $2.03 \pm 0.02$  | $-0.01 \pm 0.01$ | $-0.02 \pm 0.01$ |
| $^{32}\text{Mg}$ | 20,12  | $9.84 \pm 0.03$  | $2.37 \pm 0.03$  | $-0.21 \pm 0.02$ |
|                  |        | $3.99 \pm 0.03$  | $0.05 \pm 0.02$  | $-0.05 \pm 0.01$ |
| $^{36}\text{Ar}$ | 18,18  | $9.07 \pm 0.03$  | $1.08 \pm 0.02$  | $-0.15 \pm 0.02$ |
|                  |        | $9.07 \pm 0.03$  | $1.08 \pm 0.02$  | $-0.15 \pm 0.02$ |
| $^{40}\text{S}$  | 24,16  | $11.00 \pm 0.03$ | $5.00 \pm 0.03$  | $-0.01 \pm 0.02$ |
|                  |        | $7.57 \pm 0.04$  | $0.54 \pm 0.02$  | $-0.12 \pm 0.02$ |
| $^{42}\text{Si}$ | 28,14  | $11.77 \pm 0.02$ | $7.34 \pm 0.02$  | $0.90 \pm 0.03$  |
|                  |        | $5.79 \pm 0.03$  | $0.25 \pm 0.02$  | $-0.07 \pm 0.01$ |
| $^{42}\text{S}$  | 26,16  | $11.41 \pm 0.02$ | $6.33 \pm 0.02$  | $0.25 \pm 0.03$  |
|                  |        | $7.49 \pm 0.03$  | $0.58 \pm 0.02$  | $-0.09 \pm 0.02$ |
| $^{44}\text{S}$  | 28,16  | $11.74 \pm 0.02$ | $7.18 \pm 0.02$  | $1.06 \pm 0.03$  |
|                  |        | $7.54 \pm 0.03$  | $0.56 \pm 0.02$  | $-0.12 \pm 0.02$ |
| $^{44}\text{Ti}$ | 22,22  | $10.42 \pm 0.03$ | $3.58 \pm 0.02$  | $0.00 \pm 0.02$  |
|                  |        | $10.42 \pm 0.03$ | $3.58 \pm 0.02$  | $0.00 \pm 0.02$  |
| $^{46}\text{Ar}$ | 28,18  | $11.64 \pm 0.02$ | $7.13 \pm 0.02$  | $1.23 \pm 0.03$  |
|                  |        | $8.74 \pm 0.03$  | $1.34 \pm 0.02$  | $-0.08 \pm 0.02$ |

$N = 20$  shell is nearly completely closed at this point, and that the  $N = 28$  closure shell is reasonably robust, although approximately one neutron occupies the upper part of the  $1p0f$  shell. Coupling of the protons with the low-lying neutron excitations probably accounts for the relatively large  $B(E2)$ , without the need of invoking rotational behavior. In Table 3 we show the SMMC total Gamow-Teller ( $\text{GT}^-$ ) strength. We compare our results to those of previous truncated calculations, where available. In all cases, our results are slightly smaller than, but in good accord with, other calculations. Since we do not calculate the strength function, we do not compute  $\beta$ -decay lifetimes.

Table 3

The calculated total Gamow-Teller strength,  $GT^-$ , from this study. The results of other studies, when available, are presented for comparison.

| Nucleus          | SMMC             | Other      |
|------------------|------------------|------------|
| $^{22}\text{Mg}$ | $0.578 \pm 0.06$ |            |
| $^{30}\text{Ne}$ | $29.41 \pm 0.25$ |            |
| $^{32}\text{Mg}$ | $24.00 \pm 0.34$ |            |
| $^{36}\text{Ar}$ | $2.13 \pm 0.61$  |            |
| $^{40}\text{S}$  | $22.19 \pm 0.44$ | 22.87 [51] |
| $^{42}\text{S}$  | $28.13 \pm 0.42$ | 28.89 [51] |
| $^{42}\text{Si}$ | $40.61 \pm 0.34$ |            |
| $^{44}\text{S}$  | $34.59 \pm 0.39$ | 34.93 [51] |
| $^{44}\text{Ti}$ | $4.64 \pm 0.66$  |            |
| $^{46}\text{Ar}$ | $29.07 \pm 0.44$ | 28.84 [51] |

### 3.3.2 Heavy Sn isotopes

Effective two-hole matrix elements are calculated based on a  $Z = 50$ ,  $N = 82$  asymmetric core and with the active  $P$ -space for holes based on the  $2s_{1/2}$ ,  $1d_{5/2}$ ,  $1d_{3/2}$ ,  $0g_{7/2}$  and  $0h_{11/2}$  hole orbits. The CD-Bonn model for the NN interaction was employed [60] and all diagrams through third-order in the  $G$ -matrix were included in the evaluation of the  $\hat{Q}$ -box. Folded diagrams were again included through the method exposed above, see Refs. [4,61] for further details. The corresponding single-hole energies  $\varepsilon(d_{3/2}^+) = 0.00$  MeV,  $\varepsilon(h_{11/2}^-) = 0.242$  MeV,  $\varepsilon(s_{1/2}^+) = 0.332$  MeV,  $\varepsilon(d_{5/2}^+) = 1.655$  MeV and  $\varepsilon(g_{7/2}^+) = 2.434$  MeV are taken from Ref. [62] and the shell model calculation amounts to studying valence neutron holes outside this core. The shell model problem requires the solution of a real symmetric  $n \times n$  matrix eigenvalue equation

$$\widetilde{H} |\Psi_k\rangle = E_k |\Psi_k\rangle. \quad (79)$$

where for the present cases the dimension of the  $P$ -space reaches  $n \approx 2 \times 10^7$ . At present our basic approach in finding solutions to Eq. (79) is the Lanczos algorithm; an iterative method which gives the solution of the lowest eigenstates. This method was already applied to nuclear physics problems by Whitehead et al. in 1977. The technique is described in detail in Ref. [63], see also Ref. [64]. The results of the shell model calculation are presented in Table 4. All experimental information in the present analysis is taken from the data base of the National Nuclear Data Center at Brookhaven [65].

The isotopes above  $^{116}\text{Sn}$  (heavy Sn) are treated based on the asymmetric  $Z = 50$ ,  $N = 82$  core. This simplifies the shell model calculation, but in addition it is of interest to see how

Table 4  
Excitation spectra for the heavy Sn isotopes.

| $^{130}\text{Sn}$ |      |                |        | $^{128}\text{Sn}$ |      |                |        |
|-------------------|------|----------------|--------|-------------------|------|----------------|--------|
| $J^\pi$           | Exp. | $J^\pi$        | Theory | $J^\pi$           | Exp. | $J^\pi$        | Theory |
| (2 <sup>+</sup> ) | 1.22 | 2 <sup>+</sup> | 1.46   | (2 <sup>+</sup> ) | 1.17 | 2 <sup>+</sup> | 1.28   |
| (4 <sup>+</sup> ) | 2.00 | 4 <sup>+</sup> | 2.39   | (4 <sup>+</sup> ) | 2.00 | 4 <sup>+</sup> | 2.18   |
| (6 <sup>+</sup> ) | 2.26 | 6 <sup>+</sup> | 2.64   | (6 <sup>+</sup> ) | 2.38 | 6 <sup>+</sup> | 2.53   |
| $^{126}\text{Sn}$ |      |                |        | $^{124}\text{Sn}$ |      |                |        |
| $J^\pi$           | Exp. | $J^\pi$        | Theory | $J^\pi$           | Exp. | $J^\pi$        | Theory |
| 2 <sup>+</sup>    | 1.14 | 2 <sup>+</sup> | 1.21   | 2 <sup>+</sup>    | 1.13 | 2 <sup>+</sup> | 1.17   |
| 4 <sup>+</sup>    | 2.05 | 4 <sup>+</sup> | 2.21   | 4 <sup>+</sup>    | 2.10 | 4 <sup>+</sup> | 2.26   |
|                   |      | 6 <sup>+</sup> | 2.61   |                   |      | 6 <sup>+</sup> | 2.70   |
| $^{122}\text{Sn}$ |      |                |        | $^{120}\text{Sn}$ |      |                |        |
| $J^\pi$           | Exp. | $J^\pi$        | Theory | $J^\pi$           | Exp. | $J^\pi$        | Theory |
| 2 <sup>+</sup>    | 1.14 | 2 <sup>+</sup> | 1.15   | 2 <sup>+</sup>    | 1.17 | 2 <sup>+</sup> | 1.14   |
| 4 <sup>+</sup>    | 2.14 | 4 <sup>+</sup> | 2.30   | 4 <sup>+</sup>    | 2.19 | 4 <sup>+</sup> | 2.30   |
| 6 <sup>+</sup>    | 2.56 | 6 <sup>+</sup> | 2.78   |                   |      | 6 <sup>+</sup> | 2.86   |
| $^{118}\text{Sn}$ |      |                |        | $^{116}\text{Sn}$ |      |                |        |
| $J^\pi$           | Exp. | $J^\pi$        | Theory | $J^\pi$           | Exp. | $J^\pi$        | Theory |
| 2 <sup>+</sup>    | 1.22 | 2 <sup>+</sup> | 1.15   | 2 <sup>+</sup>    | 1.30 | 2 <sup>+</sup> | 1.17   |

successful a hole-hole effective interaction calculated with respect to  $^{132}\text{Sn}$  is.

Only some selected states are displayed. First of all, the well-known near constant  $0^+ - 2^+$  spacing is well reproduced. all the way down to  $^{116}\text{Sn}$ . Also the additional calculated

states are in very good agreement with experiment. However more detailed analysis of the results close to  $^{116}\text{Sn}$  indicates that our effective two-particle interaction has difficulties in reproducing the shell closure which is believed to occur in this region. The increase of the the  $0^+ - 2^+$  splitting is not as sharp as found experimentally, even if the phenomenon is rather weak in the case of Sn. We have observed a similar feature around  $^{48}\text{Ca}$  [4] which is generally agreed to be a good closed shell nucleus. There the deviation between theory and experiment is severe. Preliminary analysis indicates that our effective interaction may be slightly too attractive when the two particles occupy different single-particle orbits. This may be related to the radial wave functions which in our calculation are chosen to be harmonic oscillator functions.

### 3.4 Inclusion of hole-hole contributions and single-particle propagators

With the  $G$ -matrix defined according to the double-partitioned scheme we can easily solve Eq. (27) through matrix inversion. The number of hole-hole and particle-particle configurations is then rather small, typically smaller than  $\sim 100$ , and a matrix inversion is then rather trivial. Before we discuss the solution of Eq. (27), it is always instructive to consider the contributions to second order in perturbation theory, i.e., diagrams (a) and (b) of Fig. 4. The external legs can be particle states or hole states. Diagram (a) reads

$$(a) = \frac{1}{2} \sum_{pq} V_{12pqJ}^{[12]} \frac{1}{s - \varepsilon_p - \varepsilon_q} V_{pq34J}^{[12]}, \quad (80)$$

and

$$(b) = \frac{1}{2} \sum_{\alpha\beta} V_{12\alpha\beta J}^{[12]} \frac{1}{-s + \varepsilon_\alpha + \varepsilon_\beta} V_{\alpha\beta34J}^{[12]}. \quad (81)$$

We note here the minus sign in the energy denominator, since in the latter expression we are using the hole-hole term of the propagator of Eq. (28). If we use a double-partitioned  $G$ -matrix for say  $^{16}\text{O}$  and are interested in an effective valence space interaction for the  $1s0d$ -shell<sup>7</sup>, then typically the single-particle orbits of the intermediate states will be represented by states in the  $1p0f$  major shell. Hole states are then defined by single-particle states in the  $0s$  and  $0p$  shells. Clearly, the number of two-body intermediate states is rather limited. To third order we have diagrams like (c) and (d) of Fig. 4. Diagram (c) is just the third-order equivalent of Eq. (80) and reads

$$(c) = \frac{1}{4} \sum_{pqrw} V_{12pqJ}^{[12]} \frac{1}{s - \varepsilon_p - \varepsilon_q} V_{pqrwJ}^{[12]} \frac{1}{s - \varepsilon_r - \varepsilon_w} V_{rw34J}^{[12]}, \quad (82)$$

---

<sup>7</sup> This means that the labels 1234 will refer to particle states in the  $1s0d$ -shell.

while diagram (d) contains both a two-particle and a two-hole intermediate state and reads

$$(d) = \frac{1}{4} \sum_{\alpha\beta pq} V_{12pqJ}^{[12]} \frac{1}{s - \varepsilon_p - \varepsilon_q + \varepsilon_\alpha + \varepsilon_\beta} V_{pq\alpha\beta J}^{[12]} \frac{1}{s - \varepsilon_p - \varepsilon_q} V_{\alpha\beta 34J}^{[12]}. \quad (83)$$

Thus, solving Eq. (27) will then yield contributions to the effective interaction such as the above expressions.

Here we have also tacitly assumed that the energy denominators do not diverge, i.e., we have chosen an energy  $s$  so that we avoid the poles. This has always been the standard approach in calculations of shell-model effective interactions. To give an example, consider now diagram (b) and suppose that we are using harmonic oscillator wave functions. Let us also assume that the two hole states are from the  $0p$ -shell and that the valence particles are in the  $1s0d$ -shell. If we rescale the energies of the valence space to zero, then the two-hole state would yield  $-28$  MeV with an oscillator parameter  $b = 1.72$  fm. If  $s = -28$ , the denominator diverges. In this case it is rather easy to obtain the imaginary part, and even if we were to chose  $s$  different from  $-28$  MeV, the imaginary part will influence the real part of the effective interaction through dispersion relations, see e.g., Refs. [27,28,68]. It is therefore at best just a first approximation to neglect the imaginary term. Moreover, if we solve Dyson's equation for the self-energy, the single-particle energies may contain an imaginary part. Technically it is however not difficult to deal with imaginary contributions, one needs to invert a complex matrix rather than a real one. However, care must be exercised in localizing poles, see e.g., Ref. [66] for a computational approach to this problem. In our actual calculations we will also follow Ref. [66]. These technicalities will however be described elsewhere [67].

Using the double-partitioned  $G$ -matrix, we can then rewrite Eq. (27) as

$$\Gamma_{1234J}^{[12]}(s) = G_{1234J}^{[12]} + \frac{1}{2} \sum_{56} G_{1256J}^{[12]} \hat{G}^{[12]} \Gamma_{5634J}^{[12]}(s), \quad (84)$$

where  $G^{[12]}$  is just the double-partitioned  $G$ -matrix discussed above. It is also energy dependent, in contrast to  $V$ . In case we were to employ this equation for effective interactions in the  $1s0d$ -shell, the intermediate two-particle states would then come from just e.g., the  $1p0f$ -shell. This equation, which now is solved within a much smaller space than the original one spanned by the total  $Q_{pp}$ , allows clearly for computationally amenable solutions. It corresponds to the so-called *model-space approach* to the solution of the Feynman-Galitskii equations as advocated by Kuo and co-workers, see e.g., Ref. [36] for more details. Thus, a possible approach would consist of the following steps

- (i) Solve the  $G$ -matrix equation from Eq. (48) using the double-partitioning scheme.
- (ii) The next step is then to solve Eq. (27) and Dyson's equation for the self-energy.
- (iii) This scheme is iterated till self-consistency is achieved, see the discussion below.

We will however not employ this *model-space* scheme in our actual calculations. There are several reasons for not doing so.

Let us first assume that we omit the [13] and [14] channels in our iterative scheme for Eq. (84). The next iteration of Eq. (84) would then look like

$$\Gamma_{(1)}^{[12]} = \Gamma_{(0)}^{[12]} + \Gamma_{(0)}^{[12]} \hat{\mathcal{G}}^{[12]} \Gamma_{(1)}^{[12]}, \quad (85)$$

where the vertex function  $\Gamma_{(0)}^{[12]}$  is the solution of Eq. (84). However, we cannot define the “bare” vertex  $\Gamma_{(0)}^{[12]}$  to be the solution of Eq. (84) simply because then we would be double-counting contributions. Thus,  $\Gamma_{(0)}^{[12]}$  has to equal the  $G$ -matrix. The only change in Eq. (85) arises from the solution of Dyson’s equation and thereby new single-particle energies.

Let us then for the sake of simplicity assume that the single-particle energies are just the Hartree-Fock solutions. The problem we are aiming at arises at the Hartree-Fock level. In order to obtain Hartree-Fock solutions which are independent of the chosen harmonic oscillator parameter  $b$ , we typically need to include single-particle orbits from quite many major shells. Typical constraints we have found when we do so-called Brueckner-Hartree-Fock (BHF) calculations for finite nuclei is that we need at least  $2n + l \leq 20$  in order to obtain a result which is independent of the chosen  $b$ <sup>8</sup> value. The way we solve the BHF equations is to expand the new single-particle wave functions  $\psi_\lambda$ , with  $\lambda$  representing the quantum numbers  $nlj$ , in terms of harmonic oscillator wave functions, i.e.,

$$|\psi_\lambda\rangle = \sum_{\alpha=1}^{2n+l \leq 20} C_\alpha^{(\lambda)} |\phi_\alpha\rangle \quad (86)$$

where  $\phi_\alpha$  are the harmonic oscillator wave functions with quantum numbers  $\alpha = nlj$  and  $C$  are the coefficients to be varied in the Hartree-Fock calculations. The single-particle energies at the Hartree-Fock level are just

$$\varepsilon_\alpha = t_\alpha + \sum_h \langle \alpha h | G(\varepsilon_\alpha + \varepsilon_h) | \alpha h \rangle, \quad (87)$$

where the single-particle states are just those of the harmonic oscillator. The  $G$ -matrix used in the first iteration in the BHF calculation is the one given by the solution of Eq. (48). The coefficients  $C_\alpha$  can then be obtained by diagonalizing a matrix of dimension  $N \times N$ , where  $N$  is the number of single-particle orbits with the same  $lj$  values. As an example, suppose that we are considering the  $s_{1/2}$  state with  $l = 0$  and  $j = 1/2$ . With the above requirement  $2n + l \leq 20$ , we may have that  $N_{\max} = 10$ , the dimensionality being equal to the quantum number  $n$ . The way to proceed in a BHF calculation is to calculate the reference  $G$ -matrix

---

<sup>8</sup> Throughout this work our unperturbed single-particle basis par excellence will always be that of the harmonic oscillator.

$G_F$  in Eq. (49) once and for all<sup>9</sup>. Thereafter, the change in single-particle wave functions is introduced in the calculations of Eq. (48).

We see then that if we choose to do the Hartree-Fock self-consistency employing the double-partitioned  $G$ -matrix and summing the pphh diagrams as in Eq. (85), our single-particle basis will just be defined by the  $0s$ ,  $0p$ ,  $1s0d$  and  $1p0f$  shells in the case of an effective interaction in the  $1s0d$ -shell. *This is simply not enough in order to obtain a stable Brueckner-Hartree-Fock result.*

The reader could infer that why do we not perform first a BHF calculation for the  $G$ -matrix in Eq. (48), and then solve Eq. (27) and stop there. This would be in line with the abovementioned *model-space approach* of Kuo and co-workers [36]. However, if one calculates the self-energy by only including particle-particle intermediate states in the vertex function  $\Gamma$ , which is the case if we do a standard BHF calculation, one may seriously violate various sum rules, as demonstrated in Refs. [68,69]. Thus, to respect sum rules such as the conservation of number of particles constrains severely the way we solve Eqs. (27) and (29). The vertex function needs both particle-particle and hole-hole intermediate states in order to eventually satisfy e.g., the conservation of the number of particles.

Moreover, our interest lies in solving the Parquet equations. This entails simply that we perform the above self-consistency. It is therefore not only a matter of many-body aesthetics for embarking on the solution of the Parquet equations. We are also able to satisfy various sum rules. In section 4 we will also show that at every level of approximation, the solution of the equations in the [13] and [14] channels will also result in an antisymmetric vertex function in these channels.

In section 5 we will come back to the technical solution of Eq. (27) and its iterations.

#### 4 Screening corrections and vertex renormalization, the equations for the [13] and [14] channels

We start as in the previous section with the definition of the interaction vertices in the [13] and [14] channels and the corresponding integral equations. Thereafter, we discuss various approximations to these equations such as the summation of TDA and RPA diagrams. Eventually, the aim is to merge the discussion in this section and the preceding one into equations for a self-consistent scheme which combines all three channels, namely the so-called set of Parquet equations to be discussed in section 5.

---

<sup>9</sup>This matrix is typically set up in the relative and c.m. system and calculated only once and for all for  $b = 1$  fm. Other  $b$ -values involve simply a multiplication with a constant. The matrix  $G_F$  can therefore be used for other mass areas as well.

The equations for the renormalized vertex in the [13] and [14] channels have the same form as Eq. (26), namely

$$\Gamma^{[13]} = V^{[13]} + V^{[13]}(gg)\Gamma^{[13]}, \quad (88)$$

and

$$\Gamma^{[14]} = V^{[14]} + V^{[14]}(gg)\Gamma^{[14]}. \quad (89)$$

The matrix elements which enter are however defined differently and the irreducible diagrams of  $V^{[13]}$  and  $V^{[14]}$  can obviously not be the same. With irreducible in the [13] channel we will mean a diagram, which by cutting an internal particle-hole pair, cannot be separated into a piece containing the external legs 1, 3 and another piece containing 2, 4 as external legs. The definition for the irreducible vertex in the [14] channel is similar and we illustrate these differences in Fig. 9. Diagram (a) is just the lowest-order interaction in the

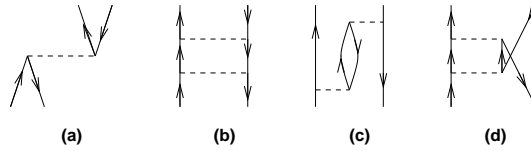


Fig. 9. Examples of irreducible and reducible diagrams in the [13] and [14] channels. See text for further details.

[13] channel and is therefore irreducible. Diagram (b) is an irreducible diagram in the [13] channel, whereas it is reducible in the [14] channel. Diagram (c) is in turn irreducible in the [14] channel and reducible in the [13] channel. Diagram (d) is an example of a diagram which is irreducible in both channels. This diagram stems from the [12] channel.

The energy variables in these channels are, following Fig. 2 and Eqs. (15) and (16),

$$t = \varepsilon_3 - \varepsilon_1 = \varepsilon_2 - \varepsilon_4, \quad (90)$$

for the [13] channel and

$$u = \varepsilon_1 - \varepsilon_4 = \varepsilon_3 - \varepsilon_2, \quad (91)$$

for the [14] channel. Defining the unperturbed particle-hole propagators in the energy representation as [36]

$$\hat{\mathcal{G}}^{[13]} = \frac{Q_{\text{ph}}^{[13]}}{t - \varepsilon_p + \varepsilon_h + \eta} - \frac{Q_{\text{hp}}^{[13]}}{t + \varepsilon_p - \varepsilon_h - \eta}, \quad (92)$$

and

$$\hat{\mathcal{G}}^{[14]} = \frac{Q_{\text{ph}}^{[14]}}{u - \varepsilon_p + \varepsilon_h + \eta} - \frac{Q_{\text{hp}}^{[14]}}{u + \varepsilon_p - \varepsilon_h - \eta} \quad (93)$$

we arrive at the following equations for the interaction vertex in these two channels

$$\Gamma_{1234J}^{[13]}(t) = V_{1234J}^{[13]} + \sum_{ph} V_{12phJ}^{[13]} \hat{\mathcal{G}}^{[13]} \Gamma_{ph34J}^{[13]}(t), \quad (94)$$

and

$$\Gamma_{1234J}^{[14]}(u) = V_{1234J}^{[14]} - \sum_{ph} V_{12phJ}^{[14]} \hat{\mathcal{G}}^{[14]} \Gamma_{ph34J}^{[14]}(u). \quad (95)$$

These equations, together with Eq. (27), can then form the basis for the first iteration in a self-consistent scheme for renormalization corrections of the Parquet type. The origin of the minus sign in Eq. (95) follows from the diagram rules [34] and will be exemplified below. A graphical view of these equations is given in Fig. 10. The reader should also keep

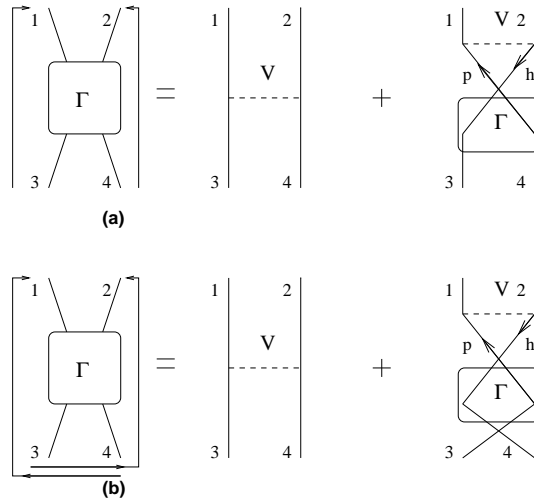


Fig. 10. (a) shows the structure of the integral equation for the interaction vertex in the [13] channel. (b) represents the integral channel for the [14] channel. The coupling order is displayed as well.

in mind the two contributions to the particle propagators of Eqs. (92) and (93). See Ref. [36] for a physical interpretation.

In this section we will omit a discussion of the self-energy corrections which arise from these channels. This will be relegated to the next section. In the nuclear case, due to the strongly repulsive short-range character of the interaction, we will have to replace in actual calculations the bare interaction in the irreducible vertices [13] and [14] with the  $G$ -matrix discussed in the previous section. Doing this entails already a first step towards the Parquet set of equations, in the sense that we are including short-range correlations from the [12] channel. Here we will however limit the discussion to expressions in terms of the interaction  $V$ . The aim is to try to recover from Eqs. (94) and (95) the familiar TDA and RPA equations and the so-called self-consistent coupled equations of Kirson [25]. The

hope is that these intermediate steps can bridge the gap between the familiar TDA, RPA and  $G$ -matrix equations and the Parquet set of equations in section 5.

#### 4.1 Screened $ph$ and $2p2h$ interactions

Here we study the screening of the particle-hole and the  $2p2h$  interactions given in Fig. 1, indicated by  $V_{ph}$  and  $V_{2p2h}$ , respectively. Before we list the final expression, it is however instructive to consider the corrections to second order in the interaction  $V$  to the  $ph$  and  $2p2h$  vertices. In Fig. 11 we display the second-order corrections to the  $ph$  diagrams of Fig.

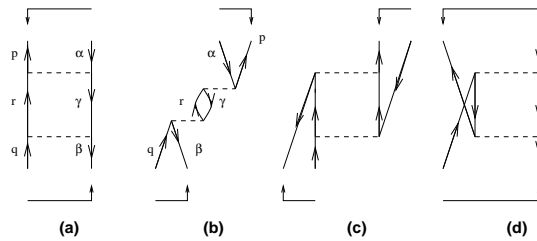


Fig. 11. Second-order perturbation theory corrections to the  $ph$  interaction vertex.

1. Diagram (a) is the core-polarization correction term to the particle-hole interaction, and corresponds to a contribution from the [14] channel, as indicated by the coupling order. The term labeled (b) corresponds to the exchange term of (a) and is coupled in the [13]-order, see also the discussion in connection with Eqs. (21) and (22). The other corrections, like (c) and (d) include particle-particle and hole-hole intermediate states, respectively. They are irreducible in both the [13] channel and the [14] channel, and can therefore enter the irreducible vertices of these two channels in later iterations. They are however not generated by various iterations of Eqs. (94) and (95). In fact, if we replace  $V$  by  $G$  in Eqs. (94) and (95), diagram (c) is already accounted for by the  $G$ -matrix. It may however be included if the double-partitioned  $G$ -matrix of the previous section is used. Let us now look at the analytical expressions in an angular momentum coupled basis for diagrams (a) and (b) of Fig. 11. Here we just include the first term of the propagators of Eqs. (92) and (93). The second terms will give rise to the  $2p2h$  contributions discussed below. In the following discussion we will also assume that the interaction  $V$  does not depend on the energy, although it is rather easy to generalize to an energy dependent interaction. Diagram (a) reads

$$(a) = - \sum_{r\gamma} (-)^{j_r+j_\gamma-J} (-)^{2j_\gamma} V_{p\gamma r\alpha J}^{[14]} \frac{1}{u + \varepsilon_\gamma - \varepsilon_r} V_{r\beta q\gamma J}^{[14]}, \quad (96)$$

The factor  $(-)^{2j_\gamma}$  stems from the opening up and recoupling of an internal particle-hole pair [34] and the phase  $(-)^{j_r+j_\gamma-J}$  is needed in order to rewrite the matrix elements in

the coupling order of Eq. (15). The general structure of Eq. (96) is just of the form  $-V_{\text{ph}}^{[14]}Q_{\text{ph}}^{[14]}/\epsilon^{[14]}V_{\text{ph}}^{[14]}$ , with  $\epsilon^{[14]} = \epsilon_q + \epsilon_\gamma - \epsilon_\beta - \epsilon_r = u + \epsilon_\gamma - \epsilon_r$  and we have defined

$$u = \epsilon_q - \epsilon_\beta = \epsilon_p - \epsilon_\alpha, \quad (97)$$

for the on-shell energy case. This is the equivalent of the energy variable of Eq. (25) in the [12] channel. Diagram (b) is in turn given by

$$(b) = \sum_{r\gamma} (-)^{j_r+j_\gamma-J} (-)^{2j_\gamma} V_{\gamma pr\alpha J}^{[13]} \frac{1}{\epsilon^{[13]}} V_{\beta r q \gamma J}^{[13]}, \quad (98)$$

and we note that the contributions are clearly different. The minus sign in Eq. (96) stems from the standard diagram rules [34]. In our use of the diagram rules below, we will omit the use of the rule for the number of external valence hole lines. In our case then, as can also be deduced from inspection of Fig. 11, diagram (a) has zero closed loops and three hole lines, giving thereby rise to a minus sign. Diagram (b) has an additional closed loop and thereby yielding the plus sign. The energy denominator is in this case

$$\epsilon^{[13]} = t + \epsilon_\gamma - \epsilon_r, \quad (99)$$

with

$$t = \epsilon_q - \epsilon_\beta = \epsilon_p - \epsilon_\alpha. \quad (100)$$

We notice, using the relations discussed in Eqs. (21) and (22), that diagram (a) is simply the exchange diagram of (b). We need however to include both diagrams in order to obtain an antisymmetric equation for the particle-hole channels which exhibits the same properties as the [12] channel shown in Eq. (24). *This is actually crucial in solving the Parquet equations. We wish namely that every iteration, with a given approximation to the vertex function  $V$ , preserves the antisymmetry property.* This point cannot be emphasized enough. Let us now see what happens to third order in the interaction. Third order corrections to the ph

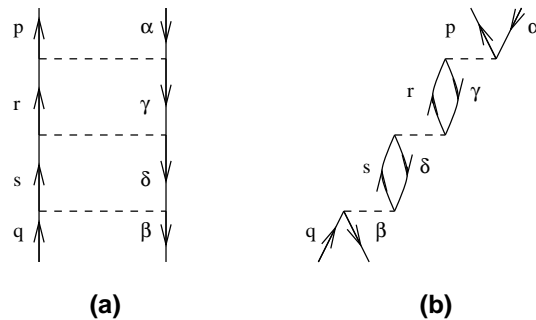


Fig. 12. Corrections beyond second order in the interaction  $V$  to the ph interaction vertex. (a) is in the [14] channel and (b) is in [13] channel.

vertices (a) and (b) involving only ph intermediate states are shown in (a) and (b) of Fig.

12, respectively. The analytical expression for the third-order contribution (a) is given by

$$(a) = \sum_{rs\gamma\delta} f V_{p\gamma r\alpha J}^{[14]} \frac{1}{u + \varepsilon_\gamma - \varepsilon_r} V_{r\delta s\gamma J}^{[14]} \frac{1}{u + \varepsilon_\delta - \varepsilon_s} V_{s\beta q\delta J}^{[14]}, \quad (101)$$

with  $f = (-)^{j_r + j_s + j_\gamma + j_\delta - 2J} (-)^{2j_\gamma + 2j_\delta}$ . This equation has the general structure

$$V_{\text{ph}}^{[14]} \frac{Q_{\text{ph}}^{[14]}}{\epsilon^{[14]}} V_{\text{ph}}^{[14]} \frac{Q_{\text{ph}}^{[14]}}{\epsilon^{[14]}} V_{\text{ph}}^{[14]}.$$

A similar expression applies to diagram (b), whose expression is

$$(b) = \sum_{rs\gamma\delta} f V_{\gamma p r\alpha J}^{[13]} \frac{1}{t + \varepsilon_\gamma - \varepsilon_r} V_{\gamma r s\delta J}^{[13]} \frac{1}{t + \varepsilon_\delta - \varepsilon_s} V_{\beta s q\delta J}^{[13]}. \quad (102)$$

It has the general structure

$$V_{\text{ph}}^{[13]} \frac{Q_{\text{ph}}^{[13]}}{\epsilon^{[13]}} V_{\text{ph}}^{[13]} \frac{Q_{\text{ph}}^{[13]}}{\epsilon^{[13]}} V_{\text{ph}}^{[13]}.$$

But these expressions have the same sign! Diagram (a) counts now 4 hole lines, and (b) counts also 4 hole lines and 2 closed loops. However, *there are three interaction terms*  $V$ , and taking the exchange term of each of these in diagram (a) leads to the desired results, namely  $(a) = -(b)$ , as it should. Thus, to third order we keep the antisymmetry property of  $\Gamma$  in the [13] and [14] channels. It is easy to see that in the [14] channel we will always have an alternating sign in front of each contribution, since every new order in perturbation theory brings a new hole line and no closed loop, and thus a new minus sign. In the [13] channel we have always one new hole line and one new closed loop for every new vertex. If we consider only the screening of the ph vertex, we can then set up a perturbative expansion in terms of the ph vertex for the vertex functions  $\Gamma^{[13]}$  and  $\Gamma^{[14]}$ . For notational economy we will skip the Pauli operators  $Q_{\text{ph, hp}}^{[ij]}$  in the discussions below. It will always be understood that the intermediate states are two-body particle-hole states,  $|\text{ph}\rangle$  or  $|\text{hp}\rangle$ . Consider e.g.,  $\Gamma^{[14]}$

$$\Gamma^{[14]} = V_{\text{ph}}^{[14]} - V_{\text{ph}}^{[14]} \frac{1}{\epsilon^{[14]}} V_{\text{ph}}^{[14]} + V_{\text{ph}}^{[14]} \frac{1}{\epsilon^{[14]}} V_{\text{ph}}^{[14]} \frac{1}{\epsilon^{[14]}} V_{\text{ph}}^{[14]} - + \dots, \quad (103)$$

which can be summed up to yield

$$\Gamma^{[14]} = V_{\text{ph}}^{[14]} - V_{\text{ph}}^{[14]} \frac{1}{\epsilon^{[14]} - V_{\text{ph}}^{[14]}} V_{\text{ph}}^{[14]} = V_{\text{ph}}^{[14]} - V_{\text{ph}}^{[14]} \frac{1}{\epsilon^{[14]}} \Gamma^{[14]}, \quad (104)$$

which is the standard TDA expression for the ph term. The corresponding expression in the [13] channel results in

$$\Gamma^{[13]} = V_{\text{ph}}^{[13]} + V_{\text{ph}}^{[13]} \frac{1}{\epsilon^{[13]}} \Gamma^{[13]}. \quad (105)$$

The signs agree with the expressions of Blaizot and Ripka [18], see chapter 15 and Eq. (15.50). The summations in both channels ensures that the final vertex is antisymmetric and the combination of the latter two equations results in the familiar TDA equations, see e.g., Ref. [36] for a matrix equation version. We next look at the  $2p2h$  matrix element and show the corresponding corrections to second order in perturbation theory in Fig. 13. If

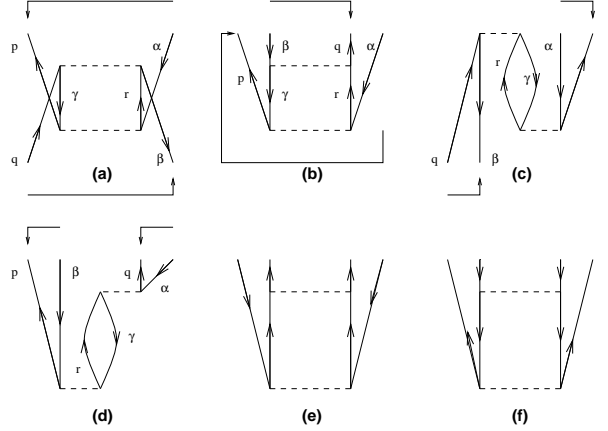


Fig. 13. Corrections to second order in  $V$  of the  $2p2h$  vertex.

we omit diagrams (e) and (f) which contain  $2p$  and  $2h$  intermediate states generated by the solutions in [12] channel, we have for diagram (a)

$$(a) = - \sum_{r\gamma} (-)^{j_r + j_\gamma - J} (-)^{2j_\gamma} V_{\gamma\beta q r J}^{[14]} \frac{1}{-u + \varepsilon_\gamma - \varepsilon_r} V_{pr\gamma\alpha J}^{[14]}, \quad (106)$$

with the general structure

$$-V_{2p2h}^{[14]} \frac{1}{\epsilon^{[14]}} V_{2p2h}^{[14]}. \quad (107)$$

Note well the minus sign in front of  $u$ . The contribution from the propagator can in this case be retraced to the second term of the propagator of Eq. (93). Diagram (a) follows the coupling order of the [14] channel. It is also easy to see that diagram (b) is given by

$$(b) = - \sum_{r\gamma} (-)^{j_r + j_\gamma - J} (-)^{2j_\gamma} V_{\gamma q \beta r J}^{[14]} \frac{1}{-u + \varepsilon_\gamma - \varepsilon_r} V_{pr\gamma\alpha J}^{[14]}, \quad (108)$$

and has the structure

$$-V_{ph}^{[14]} \frac{1}{\epsilon^{[14]}} V_{2p2h}^{[14]}. \quad (109)$$

Similarly, if we now move to the [13] channel we have the following expressions

$$(c) = \sum_{r\gamma} (-)^{j_r + j_\gamma - J} (-)^{2j_\gamma} V_{\beta\gamma q r J}^{[13]} \frac{1}{-t + \varepsilon_\gamma - \varepsilon_r} V_{qp\gamma\alpha J}^{[13]}, \quad (110)$$

and

$$(d) = \sum_{r\gamma} (-)^{j_r+j_\gamma-J} (-)^{2j_\gamma} V_{\gamma q r \alpha J}^{[13]} \frac{1}{-t + \varepsilon_\gamma - \varepsilon_r} V_{p r \beta \gamma J}^{[13]}, \quad (111)$$

with the general structure

$$V_{2p2h}^{[13]} \frac{1}{\epsilon^{[13]}} V_{2p2h}^{[13]}, \quad (112)$$

and

$$V_{ph}^{[13]} \frac{1}{\epsilon^{[13]}} V_{2p2h}^{[13]}, \quad (113)$$

respectively. Diagram (c) is just the exchange of (a) and includes two 2p2h vertices, while diagram (d) is the exchange of diagram (b) and includes a ph vertex multiplied with a 2p2h vertex. We note again that the antisymmetry is ensured at a given order in the interaction only if we include the corrections at the same level in both channels.

One can then easily sum up higher-order corrections to the 2p2h diagrams as well in both channels. The inclusion of the backward going particle-hole pair in the propagators of Eqs. (92) and (93) ensures thus that we will also sum to infinite order 2p2h corrections. This leads ultimately to the familiar RPA equations, see e.g., Refs. [26,36].

A closer inspection of Eqs. (108) and (111) shows that if we only include ph vertices, we could resum these corrections to infinite order for the 2p2h vertex by observing that the structure of such diagrams would be of the form (e.g., in the [14] channel )

$$\Gamma_{2p2h}^{[14]} = V_{2p2h}^{[14]} - V_{ph}^{[14]} \frac{1}{\epsilon^{[14]}} V_{2p2h}^{[14]} + V_{ph}^{[14]} \frac{1}{\epsilon^{[14]}} V_{ph}^{[14]} \frac{1}{\epsilon^{[14]}} V_{2p2h}^{[14]} + \dots, \quad (114)$$

which can be summed up to yield

$$\Gamma_{2p2h}^{[14]} = V_{2p2h}^{[14]} - V_{ph}^{[14]} \frac{1}{\epsilon^{[14]} - V_{ph}^{[14]}} V_{2p2h}^{[14]}, \quad (115)$$

and similarly for the [13] channel, but with a plus sign. The modification discussed in Eqs. (104) and (115) serve to modify the propagation of a particle-hole pair and have normally been termed for propagator renormalizations, as can easily be seen from Eqs. (104) and (115) where the propagation of a free particle-hole pair is modified by the presence of the interaction  $V$  in the energy denominator. Other important processes which can affect e.g., various polarization terms are those represented by so-called vertex renormalizations, a term originally introduced by Kirson and Zamick [70]. These authors studied the renormalizations of the 2p1h and 2h1p vertices as well, see also Kirson [25] and Ellis and Osnes [26] for further discussions. We will therefore end the discussion in this section by looking at such renormalizations.

## 4.2 Further renormalizations

In the previous subsection we dealt mainly with what has conventionally been labelled for propagator renormalizations. We will therefore extend the standard TDA and RPA scheme by looking at further ways of renormalizing interaction vertices. The approach discussed here follows Kirson [25]. Extensions were made later by Ellis and Goodin [71] and Ellis, Mavrommatis and Mütter [32]. We will limit the discussion here to the scheme of Kirson. We start therefore with the contributions to second order to the 2p1h vertex<sup>10</sup>. These

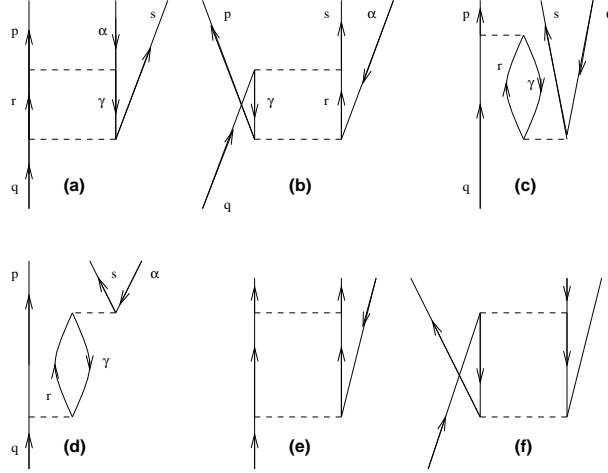


Fig. 14. The corrections to second order in  $V$  of the 2p1h vertex.

contributions are shown in Fig. 14. Diagram (a) consists of a 2p1h vertex multiplied with a ph vertex whereas (b) stems from the multiplication of a 2p2h vertex with a 2p1h vertex. They both contain a particle-hole pair as an intermediate state and follow the coupling order of the [14] channel. The exchange diagram of (b) is given by (c), while that of (a) is diagram (d). Diagrams (e) and (f) represent contributions from the [12] channel and are irreducible in both particle-hole channels. Before we sketch the general structure of the renormalization procedure of Kirson, it is instructive to consider again the equations to second order in perturbation theory, as the general expressions can be deduced from inspection of these diagrams. Diagram (a) is

$$(a) = \sum_{r\gamma} (-)^{j_r + j_\gamma - J} (-)^{2j_\gamma} V_{p\gamma r\alpha J}^{[14]} \frac{1}{u + \varepsilon_\gamma - \varepsilon_r} V_{rsq\gamma J}^{[14]}, \quad (116)$$

and the plus sign stems from the diagram rules [34], i.e., we have two hole lines and no closed loop. The propagator is that arising from the first term in Eq. (93). The general structure is

$$V_{\text{ph}}^{[14]} \frac{1}{\varepsilon^{[14]}} V_{2\text{p1h}}^{[14]}. \quad (117)$$

<sup>10</sup> The discussion here applies to the other interaction vertices discussed in Fig. 1.

Diagram (b) reads

$$(b) = \sum_{r\gamma} (-)^{j_r+j_\gamma-J} (-)^{2j_\gamma} V_{pr\gamma\alpha J}^{[14]} \frac{1}{-u + \varepsilon_\gamma - \varepsilon_r} V_{\gamma s q r J}^{[14]}, \quad (118)$$

with the following structure

$$V_{2p1h}^{[14]} \frac{1}{\varepsilon^{[14]}} V_{2p2h}^{[14]}. \quad (119)$$

In this case the propagator stems from the second term in Eq. (93). Similar equations arise for e.g., the 2h1p vertices of Fig. 1.

Before we write down the self-consistent equations of Kirson [25], let us assume that we can approximate the 2p1h vertex in the [14] channel by the first order term and diagrams (a) and (b). This renormalized vertex, which we here label  $\tilde{V}_{2p1h}$ , is then given by

$$\tilde{V}_{2p1h} \approx V_{2p1h}^{[14]} + V_{ph}^{[14]} \frac{1}{\varepsilon^{[14]}} V_{2p1h}^{[14]} + V_{2p1h}^{[14]} \frac{1}{\varepsilon^{[14]}} V_{2p2h}^{[14]}. \quad (120)$$

If we now allow for the screening to infinite order of the ph vertex given by Eq. (104) and replace the 2p2h vertex in the above equation with Eq. (115) we obtain the following renormalization of the 2p1h vertex

$$\tilde{V}_{2p1h} = V_{2p1h}^{[14]} + V_{ph}^{[14]} \frac{1}{\varepsilon^{[14]} - V_{ph}^{[14]}} V_{2p1h}^{[14]} + V_{2p1h}^{[14]} \frac{1}{\varepsilon^{[14]} - V_{ph}^{[14]}} V_{2p2h}^{[14]}. \quad (121)$$

A similar equation applies to the 2h1p vertex of Fig. 1 and for the [13] channel. Eqs. (104), (115) and (121) form then the starting point for the approach of Kirson [25]. Examples of diagrams which can be obtained through the iterative solution of Eqs. (104), (115) and (121) are given in Fig. 15.

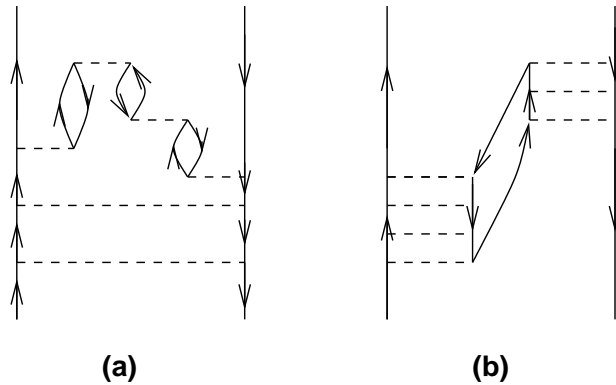


Fig. 15. Examples of diagrams which can arise from Kirson's self-consistent equations.

The question now is however how to relate Eqs. (104), (115) and (121) with those from Eqs. (94) and (95). This is rather trivial if we recall that the labels 1234 can, as was also

discussed in section 2, represent whatever single-particle states, either holes or particles. Thus,  $V_{1234}$  can represent a 2p1h, 2h1p, 2p2h, 2p, 2h or a ph vertex. This means that, due to the choice of propagators in Eqs. (92) and (93) equations like Eq. (121) are already inherent in Eqs. (94) and (95). If we e.g., approximate Eq. (95) to second order in the interaction  $V$  and let the single-particle labels 1234 represent a 2p1h interaction vertex, we immediately reobtain Eq. (120). If we let 1234 represent a 2p2h vertex, we find to second order diagrams (a)-(d) of Fig. 13.

Till now we have however refrained from discussing the contributions from the [12] channel, examples were only shown in (c) and (d) of Fig. 11, (e) and (f) of Figs. 13 and 14. These diagrams cannot be generated by simply iterating the equations for the [13] and [14] channels, but they could enter as contributions to the irreducible vertex in the [13] and [14] channels from the first iteration in the [12]-channel. We see thus the emerging contour of an iterative scheme. The crucial point is however how to perform the next iteration of say Eqs. (104), (115) and (121) or Eqs. (94), (95) and (27) from the [12] channel. The question is how do we include the results from the first iteration into the next one, i.e., how to modify the bare vertices  $V^{[13]}$  and  $V^{[14]}$  in e.g., Eqs. (94) and (95) in order to obtain an effective interaction for the shell model. We have also not addressed how to deal with the solution of Dyson's equation for the one-body Green's function. We mention also that Ellis and Goodin [71] included pp correlations, i.e., terms from the [12] channel such as diagram (e) of Fig. 14, as well when they considered the screening of the 2p1h and 2h1p vertices. Furthermore, as already mentioned in the introduction the authors of Refs. [32,33] extended the pp RPA to include the particle-hole (ph) RPA, though screening of the 2p1h and 2h1p vertices was not included. In Ref. [33] however, a study with self-consistent single-particle energies was also performed. These works represent thus a first serious step towards the solution of the Parquet equations, i.e., a many-body scheme which solves self-consistently the equations in the [12], [13] and [14] channels, with the addition of the self-consistent evaluation of the self-energy. It ought also to be mentioned that one of the really first applications for nuclear systems was performed in a series of papers by Dickhoff and Mütter and co-workers [72] for nuclear matter. These authors actually performed the first iteration of the three channels.

Such a synthesis of the equations for the three channels discussed here will be made in the next section.

## 5 Effective interactions for finite nuclei from Parquet diagrams

The equations we discussed in the two previous sections can be generalized in matrix form as

$$\Gamma = \Gamma^{[ij]} + \Gamma^{[ij]} \hat{\mathcal{G}}^{[ij]} \Gamma, \quad (122)$$

where obviously  $[ij]$  represents a given channel,  $\hat{\mathcal{G}}^{[ij]}$  is the particle-particle, or hole-hole or particle-hole propagator. The propagator is a product of two single-particle propagators  $g$  which we do not specify any further here. They are defined by the solution of Dyson's equation in Eq. (29). The irreducible vertices must appear in the solution of the self-energy, and conversely, the self-energy must appear in all single-particle propagators within the expressions for the three channels [12], [13] and [14].

For all of our practical purposes, the irreducible vertex used in all channels is the so-called free  $G$ -matrix defined in Eq. (49). We will explain more why this is our preferred choice below. Let us now define the contribution from the [12], [13] and [14] channels following Ref. [17]. Eq. (27) is then rewritten as

$$L = \Gamma^{[12]} - G_F, \quad (123)$$

where obviously  $L$  stands for ladder and if we neglect hole-hole terms in Eq. (27) we obtain

$$L = \Delta G = G - G_F, \quad (124)$$

that is the ladder corrections beyond first order in our irreducible vertex function  $G_F$ , as discussed in section 3. The ladder term can then be rewritten as

$$L = G_F \hat{\mathcal{G}}^{[12]} G_F + G_F \hat{\mathcal{G}}^{[12]} L. \quad (125)$$

In a similar way we can define the diagrams beyond first order in the particle-hole channel as

$$R^{[13]} = \Gamma^{[13]} - G_F, \quad (126)$$

and

$$R^{[14]} = \Gamma^{[14]} - G_F, \quad (127)$$

where  $G_F$  now is coupled in either the [13] or [14] way. Rewriting  $R^{[ij]}$ , where  $R$  refers to ring diagrams, we obtain

$$R^{[ij]} = G_F \hat{\mathcal{G}}^{[ij]} G_F + G_F \hat{\mathcal{G}}^{[ij]} R^{[ij]}, \quad (128)$$

where  $ij$  stands for either [13] or [14]. The equation for the vertex function  $\Gamma$  in Eq. (122) becomes then

$$\Gamma = G_F + L + R^{[13]} + R^{[14]}. \quad (129)$$

*Note here that the vertex  $\Gamma$  can be represented in the coupling order of any of the above channels. Our convention is that of the [12] channel.*

If Eqs. (125) and (128) define the first iteration, it should be fairly obvious to see that the next iteration would be

$$L = (G_F + R^{[13]} + R^{[14]}) \hat{\mathcal{G}}^{[12]} (G_F + R^{[13]} + R^{[14]}) + (G_F + R^{[13]} + R^{[14]}) \hat{\mathcal{G}}^{[12]} L, \quad (130)$$

where the contributions  $R^{[13]} + R^{[14]}$  are recoupled according to the coupling order of the 12-channel. These contributions are irreducible in the [12] channel. Similarly, for the rings we have

$$R^{[13]} = (G_F + L + R^{[14]}) \hat{\mathcal{G}}^{[13]} (G_F + L + R^{[14]}) + (G_F + L + R^{[14]}) \hat{\mathcal{G}}^{[13]} R^{[14]}, \quad (131)$$

and

$$R^{[14]} = (G_F + L + R^{[13]}) \hat{\mathcal{G}}^{[14]} (G_F + L + R^{[13]}) + (G_F + L + R^{[13]}) \hat{\mathcal{G}}^{[14]} R^{[14]}. \quad (132)$$

Our scheme for calculating  $\Gamma$  will be an iterative one based on Eqs. (129)-(132) and the solution of Dyson's equation for the single-particle propagator. This set of equations will then yield the two-body Parquet diagrams. Relating the above equations to the discussions of sections 3 and 4, it is rather easy to see that the  $G$ -matrix, TDA, RPA and Kirson's screening scheme are contained in Eqs. (129)-(132) .

### 5.1 *Petit Parquet*

The aim here is to present a numerically viable approach to the Parquet equations. Here we will limit ourself to just sketch the structure of the solution, more technical details will be represented elsewhere [67].

The iterative scheme starts with the solution of Eq. (27). The bare vertex which is irreducible in all three channels is the so-called free  $G$ -matrix  $G_F$  defined in Eq. (49). Let us use the identity from Ref. [37] and rewrite the vertex function  $\Gamma^{[12]}$  as

$$\Gamma^{[12]} = G_F + G_F \left( \frac{Q^{[12]}}{s - H_0} - \frac{1}{s - H_0} \right) \Gamma^{[12]}, \quad (133)$$

where

$$G_F = V + V \frac{1}{s - H_0} G_F.$$

We define then  $Q^{[12]} = Q_{pp} + Q_{hh}$  and use Eq. (47) to rewrite  $Q_{pp}$  and obtain

$$\Gamma_{(0)}^{[12]} = G_F - G_F \left( \frac{Q_{hh}}{s - H_0} + \frac{1}{s - H_0} \tilde{P} \frac{1}{\tilde{P}(s - H_0)^{-1} \tilde{P}} \tilde{P} \frac{1}{s - H_0} \right) \Gamma_{(0)}^{[12]}. \quad (134)$$

The subscript (0) means that this is just the first iteration. The single-particle energies are the unperturbed harmonic oscillator energies.

Since we will always deal with real single-particle energies, the two-body propagators of Eqs. (28), (92) and (93) will have the same expressions except for the fact that the single-particle energies get renormalized after each iteration. This means that the denominators in  $G_F$ ,  $\Gamma_{(0)}^{[12]}$  and subsequent iterations and the expressions for the ring diagrams from the [13] and [14] channels, can be rewritten via the simple relation

$$\frac{1}{s \pm i\eta} = P \frac{1}{s} \mp i\pi\delta(s). \quad (135)$$

With this caveat, we can in turn obtain the real and imaginary parts of all matrices involved.

The first step in our calculations is to evaluate  $G_F$ . It is calculated in momentum space for a series of starting energies (typically  $\sim 30$ ). The principal value integral from Eq. (135) is solved using Kowalski's [73] method. This method ensures a numerical stable treatment with large numbers of mesh points in momentum space. From the principal value integral we can in turn define the real and imaginary part of  $G_F$ , see e.g., Ref. [28] for technical details. The matrix  $G_F$  is solved only once and transformed to a harmonic oscillator basis in the lab from the relative and center of mass system, see Ref. [4] for details.

The second step is to solve Eq. (134), which is now a complex equation. Since the number of two-hole states is rather limited, typically  $\leq 100$  for a given  $J$  even for heavy nuclei like Pb, the major problem in the matrix inversion of Eq. (134) resides in the dimensionality of  $\tilde{P}$  discussed in section 3. What conditions our truncation of  $\tilde{P}$  and the number  $n_3$ , is dictated by the Brueckner-Hartree-Fock (BHF) independence on the chosen oscillator parameter  $b$ . This choice leads to the inclusion of more than ten major shells in the computation of the  $G$ -matrix. For a given  $J$  value, the total number of two-body states needed can then be of the order  $\sim 10^4$ .

*Our first approximation* is therefore to truncate the available space of single-particle states to be within  $\sim 10 - 20$  major shells. The choice being conditioned by the BHF criteria and the possibility to store these large matrices in the RAM of available computing facilities. If we choose to use a double-partitioned model space, we need to sum up further diagrams with particle-particle intermediate states.

These two steps lead then to the first iteration of the ladders, i.e.,

$$L_{(0)} = \Gamma_{(0)}^{[12]} - G_F. \quad (136)$$

It contains both hole-hole and particle-particle intermediate states and is a complex matrix. The external single-particle legs can be particles or holes. Only unperturbed single-particle energies enter the definition of the two-body propagators.

The third step is to calculate the first iteration for the rings, namely

$$R_{(0)}^{[13]} = (G_F + L_{(0)}) \hat{\mathcal{G}}^{[13]} (G_F + L_{(0)}) + (G_F + L_{(0)}) \hat{\mathcal{G}}^{[13]} R_{(0)}^{[13]}, \quad (137)$$

and

$$R_{(0)}^{[14]} = (G_F + L_{(0)}) \hat{\mathcal{G}}^{[14]} (G_F + L_{(0)}) + (G_F + L_{(0)}) \hat{\mathcal{G}}^{[14]} R_{(0)}^{[14]}. \quad (138)$$

The equations for  $L$  and  $R$  are all defined within a truncated Hilbert space. They can therefore be recast into matrix equations of finite dimensionality. Recall also that we need to recouple the contribution from the [12] into the relevant ones for the [13] and [14] channels. This is done employing Eqs. (15) and (16). With these contributions, we can now obtain the vertex function  $\Gamma$  after the first interaction

$$\Gamma_{(0)} = G_F + L_{(0)} + R_{(0)}^{[13]} + R_{(0)}^{[14]}. \quad (139)$$

The fourth step is to compute the self-energy and thereby obtain new single-particle energies. In so doing, care has to be exercised in order to avoid double-counting problems. A thorough discussion of this topic can be found in Ref. [17]. More details will also be presented in Ref. [67]. Through dispersion relations [28] we can in turn obtain the real part of the self-energy and our single-particle energies will be approximated by

$$\varepsilon_\alpha = t_\alpha + \text{Re}\Sigma_\alpha. \quad (140)$$

This is *our second approximation*. The new single-particle wave functions of Eq. (86) are obtained by diagonalizing a matrix of dimension  $n_\alpha \times n_\alpha$ ,  $n_\alpha$  the quantum number  $n$  of the single-particle state  $\alpha$ .

The fifth step is to repeat steps 1-4 with the new single-particle energies till a predetermined self-consistency is obtained. But now the rings have to be included in all equations, i.e., we solve Eqs. (129)-(132).

The final vertex  $\Gamma$  can then be used to define a new effective interaction to be applied in shell model studies, where many more diagrams are considered than in present state of the art calculations, see e.g., Fig. 8 of Ref. [17] for a list of diagrams to sixth order entering the definition of the irreducible vertex  $\Gamma$ .

## 6 Perspectives

The reader should always keep in mind that the many-body scheme we have focussed on is only one of several possible ways of calculating effective interactions. Other methods are also discussed in this volume.

The aim of this work has however been to show how one can practically implement the Parquet equations in order to obtain effective interactions for the nuclear shell model. The emphasis here has been to connect these equations with state of the art approaches to effective interactions. Thus, how to recover the standard  $G$ -matrix equation and the TDA and RPA equations from the Parquet equations has been outlined. Applications of this many-body scheme will be presented elsewhere [67], although in depth discussions and applications of both the  $G$ -matrix, folded diagrams and other perturbative resummations can be found in e.g., Refs. [4,26]. There are also subtle technical details which deal with double-counting problems in the outlined iterative Parquet scheme that we have left out, due to space limits, in the discussion. We take the liberty here to refer to e.g., Refs. [17,19]. They will also be discussed in Ref. [67].

In the scheme we have sketched, there are obviously other important many-body contributions at the two-body level which cannot be generated by the two-body Parquet equations. We have also omitted any discussion of three-body terms. Such terms could be generated if we were to solve the three-body Parquet equations, see Lande and Smith [17]. An implementation of the three-body Parquet equations is in progress. Three-body terms, as also mentioned in the introduction, are believed to be important, it should just suffice to mention studies of the Triton [74]. With two-body forces only one is also not able to reproduce properly the nuclear matter saturation point [75]. In connection with three-body contributions one has to carefully distinguish between three-body forces and effective three-body interactions. To understand this point consider the following arguments from studies of infinite nuclear matter and finite nuclei. The last three years have seen quite some advances in many-body studies of dense infinite matter, see e.g., Refs. [75–77] for recent surveys. These results can be summarized as follows. Firstly, new  $NN$  interactions such as the CD-Bonn potential [60], different Nijmegen interactions [78] and the recent Argonne  $V_{18}$  interaction [79] all fit the set of scattering data of the Nijmegen group with a  $\chi^2$  per datum close to 1. All these interactions, when applied to calculations of the equation of state (EoS), yield essentially similar equations of state up to densities of 3 – 4 nuclear matter saturation density for both pure neutron matter and  $\beta$ -stable matter when the non-relativistic lowest-order Brueckner theory (LOB) is used. Other properties like the symmetry energy and proton fractions do also show a similar quantitative agreement, see Ref. [76] for more details. Secondly, the inclusion of more complicated many-body terms at the two-body [75] level does not alter this picture and even the recent summation of three-hole line diagrams of Baldo and co-workers [77] results in an EoS which is close to LOB when a continuous choice is used for the single-particle energies in matter [77]. The latter are examples of effective three-body contributions. These findings are also in line with recent works on the energy of pure neutron drops, where three-body clusters are included [80], and large-scale shell-model calculations of Sn isotopes including effective three-body interactions [81]. Differences do however occur when one introduces real three-body forces. These are necessary in order to reproduce the saturation properties of nuclear matter [75] and the binding energy of light nuclei [24].

The reader may then eventually ask why do we bother at all to solve the two-body set of Parquet equations when most likely these new effective interactions will not cure any of the problems seen in shell model studies or nuclear matter. One needs at least to include some realistic three-body force and thereby to solve the three-body Parquet equations. The problem however with real three-body forces is that presently we have no serious candidates which exhibit the same level of quality and sophistication as the  $NN$  interactions mentioned above. The introduction of such forces lead therefore to strong model dependencies. Moreover, to assess properly many-body terms at the two-body level is an important, and not yet solved, problem per se. The Parquet equations allow one also to include in a self-consistent way several many-body terms, fulfill crossing symmetries and satisfy certain sum rules. In addition, the Green's function formalism can be taylorred for finite temperatures. This is clearly of interest for studies of infinite matter at finite temperature, such as e.g., dense matter occuring in a newly born neutron star. The application of the Parquet equation in nuclear and neutron matter will also allow for a consistent treatment of screening effects relevant for the pairing problem. Such work is in progress.

### *Acknowledgements*

I have greatly benefitted from many discussions on Parquet theory with Andy Jackson. Moreover, many interactions with David Dean, Paul Ellis, Torgeir Engeland, Tom Kuo, Herbert Mütter, Artur Polls, Eivind Osnes and Andres Zuker have hopefully matured some of the ideas exposed, although any eventual flaw(s) is(are) obviously to be retraced to the author.

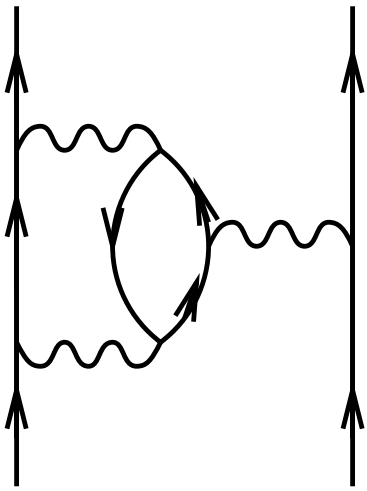
### References

- [1] K. Suzuki, R. Okamoto and H. Kumagai, Nucl. Phys. **A580** (1994) 213; K. Suzuki and R. Okamoto, Prog. Theor. Phys. **92** (1994) 1045; *ibid.* **93** (1995) 905; K. Suzuki and R. Okamoto, this volume.
- [2] B.H. Brandow, Rev. Mod. Phys. **39** (1967) 771.
- [3] T.T.S. Kuo and E. Osnes, *Folded-Diagram Theory of the Effective Interaction in Atomic Nuclei*, Springer Lecture Notes in Physics, (Springer, Berlin, 1990) Vol. **364**; T.T.S. Kuo, *Lecture Notes in Physics; Topics in Nuclear Physics*, eds. T.T.S. Kuo and S.S.M. Wong, (Springer, Berlin, 1981) Vol. **144**, p. 248.
- [4] M. Hjorth-Jensen, T.T.S. Kuo and E. Osnes, Phys. Rep. **261** (1995) 125.
- [5] I. Lindgren and J. Morrison, *Atomic Many-Body Theory*, (Springer, Berlin, 1985); I. Lindgren, J. Phys. B: At. Mol. Opt. Phys. **24** (1991) 1143.

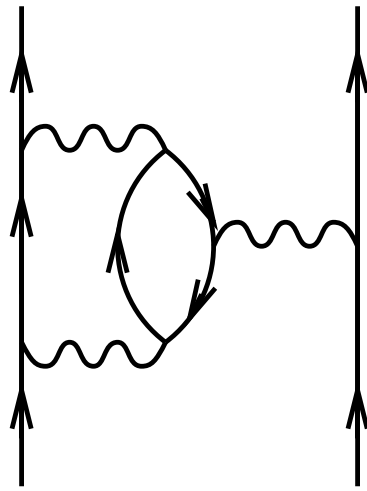
- [6] K. Suzuki, Prog. Theor. Phys. **68** (1982) 1627; K. Suzuki and R. Okamoto, Prog. Theor. Phys. **75** (1986) 1388; ibid. **76** (1986) 127.
- [7] J. Arponen, Phys. Rev. **A55** (1997) 2686.
- [8] H. Kümmel and K.H. Lührmann, Nucl. Phys. **A191** (1972) 525.
- [9] H. Kümmel and K.H. Lührmann, Nucl. Phys. **A194** (1972) 225.
- [10] J.G. Zabolitzky, Nucl. Phys. **A228** (1974) 285.
- [11] H. Kümmel, K.H. Lührmann and J.G. Zabolitzky, Phys. Rep. **36** (1977) 1.
- [12] R.F. Bishop, E. Buendia, M.F. Flynn and R. Guardiola, J. Phys. G: Nucl. Part. Phys. **17** (1991) 857; ibid. **18** (1992) 1157; ibid. **19** (1993) 1663; R. Guardiola, P.I. Moliner, J. Navarro, R.F. Bishop, A. Puente and N.R. Walet, Nucl. Phys. **A609** (1996) 218; R.F. Bishop and R. Guardiola, this volume.
- [13] J.H. Heisenberg and B. Mihaila, nucl-th/9802031; B. Mihaila and J.H. Heisenberg, nucl-th/9802021; nucl-th/9802032.
- [14] C. de Dominicis and P.C. Martin, J. Math. Phys. **5** (1964) 14.
- [15] B. Roulet, F. Gavoret and P. Nozieres, Phys. Rev. **178** (1969) 1072.
- [16] S. Babu and G.E. Brown, Ann. Phys. **78** (1973) 1.
- [17] A.D. Jackson, A. Lande and R.A. Smith, Phys. Rep. **86** (1982) 55; A. Lande and R.A. Smith, Phys. Rev. **A45** (1992) 913 and references therein.
- [18] J.P. Blaizot and G. Ripka, *Quantum theory of finite systems*, (MIT press, Cambridge, USA, 1986), chapter 15.
- [19] N.E. Bickers and D.J. Scalapino, Ann. Phys. **193** (1989) 206; N.E. Bickers and S.R. White, Phys. Rev. **B43** (1991) 8044; N.E. Bickers and D.J. Scalapino, Phys. Rev. **B46** (1992) 8050.
- [20] J. Yeo and M.A. Moore, Phys. Rev. **B54** (1996) 4218.
- [21] A.T. Zheleznyak, V.M. Yakovenko and I.E. Dzyaloshinskii, Phys. Rev. **B55** (1997) 3200.
- [22] A. Fabrocini, F. Arias de SAVEDRA, G. C o and P. Folgarait, Phys. Rev. **C57** (1998) 1668; A. Fabrocini and S. Fantoni, this volume.
- [23] S.E. Koonin, D.J. Dean and K.-H. Langanke, Phys. Rep. **278** (1997) 1.
- [24] B.S. Pudliner, V.R. Pandharipande, J. Carlson, S.C. Pieper and R.B. Wiringa, Phys. Rev. **C56** (1997) 1720 and references therein.
- [25] M.W. Kirson, Ann. Phys. **66** (1971) 624; ibid. **68** (1971) 556; ibid. **82** (1974) 345.
- [26] P.J. Ellis and E. Osnes, Rev. Mod. Phys. **49** (1977) 777.
- [27] A. Ramos, PhD. Thesis, University of Barcelona, 1988, unpublished.

- [28] A. Ramos, A. Polls and W.H. Dickhoff, Nucl. Phys. **A503** (1989) 1.
- [29] S.D. Yang, J. Heyer and T.T.S. Kuo, Nucl. Phys. **A448** (1986) 420.
- [30] H.Q. Song, S.D. Yang and T.T.S. Kuo, Nucl. Phys. **A462** (1987) 491.
- [31] H.A. Mavromatis, H. Müther, T. Taigel and T.T.S. Kuo, Nucl. Phys. **A470** (1987) 185.
- [32] H.A. Mavromatis, P.J. Ellis and H. Müther, Nucl. Phys. **A530** (1991) 251.
- [33] E. Heinz, H. Müther and H.A. Mavromatis, Nucl. Phys. **A587** (1995) 77.
- [34] T.T.S. Kuo, J. Shurpin, K.C. Tam, E. Osnes and P.J. Ellis, Ann. Phys. **132** (1981) 237.
- [35] W.H. Dickhoff and H. Müther, Rep. Prog. Phys. **55** (1992) 1947.
- [36] T.T.S. Kuo and Y. Tzeng, Int. J. Mod. Phys. **E3** (1994) 523.
- [37] H.A. Bethe, B.H. Brandow and A.G. Petschek, Phys. Rev. **129** (1963) 225.
- [38] E.M. Krenciglowa, C.L. Kung, T.T.S. Kuo and E. Osnes, Ann. Phys. **101** (1976) 154.
- [39] S.Y. Lee and K. Suzuki, Phys. Lett. **B 91** (1980) 79; K. Suzuki and S.Y. Lee, Prog. Theor. Phys. **64** (1980) 2091.
- [40] J. Des Cloizeaux, Nucl. Phys. **20** (1960) 321.
- [41] T.T.S. Kuo, P.J. Ellis, J. Hao, Z. Li, K. Suzuki, R. Okamoto and H. Kumagai, Nucl. Phys. **A560** (1993); P. Navratil, H.B. Geyer and T.T.S. Kuo, Phys. Lett. **B315** (1993) 1.
- [42] D.J. Dean, M.T. Ressel, M. Hjorth-Jensen, S.E. Koonin, K. Langanke, and A.P. Zuker, submitted to Phys. Rev. **C**.
- [43] T. Motobayashi et al., Phys. Lett. B **B 346** (1995) 9.
- [44] H. Scheit et al., Phys. Rev. Lett. **77** (1996) 3967.
- [45] T. Glasmacher et al., Phys. Lett. **B395** (1997) 163.
- [46] T.R. Werner et al., Nucl. Phys. **A597** (1996) 327.
- [47] X. Campi, H. Flocard, A.K. Kerman and S.E. Koonin, Nucl. Phys. **A251** (1975) 193.
- [48] E.K. Warburton, J.A. Becker and B.A. Brown, Phys. Rev. **C41** (1990) 1147.
- [49] A. Poves and J. Retamosa, Nucl. Phys. **A571** (1994) 221.
- [50] N. Fukunishi, T. Otsuka and T. Sebe, Phys. Lett. **B296** (1992) 279.
- [51] J. Retamosa, E. Caurier, F. Nowacki and A. Poves, Phys. Rev. **C55** (1997) 1266.
- [52] E. Caurier, F. Nowacki, A. Poves and J. Retamosa, Phys. Rev. **C58** (1998) 2033.
- [53] S.E. Koonin, D.J. Dean, and K. Langanke, Ann. Rev. Nucl. Part. Sci. **47** (1997) 463.

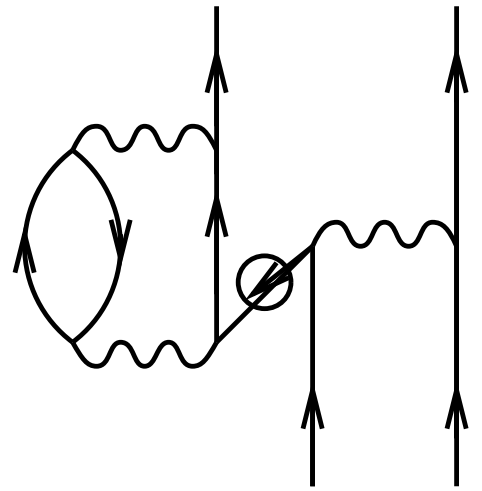
- [54] G.H. Lang, C.W. Johnson, S.E. Koonin and W.E. Ormand, Phys. Rev. **C48** (1993) 1518.
- [55] A. Abzouzi, E. Caurier, and A.P. Zuker, Phys. Rev. Lett. **66** (1991) 1134.
- [56] J. Duflo and A. P. Zuker, submitted to Phys. Rev. Lett.
- [57] P.M. Endt, Nucl. Phys. **A521** (1990) 1.
- [58] S. Raman et al., At. Data and Nucl. Data Tab. **36** (1987) 1.
- [59] A. Poves and J. Retamosa, Phys. Lett. **B184** (1987) 311.
- [60] R. Machleidt, F. Sammarruca, and Y. Song, Phys. Rev. **C53** (1996) R1483.
- [61] A. Holt, T. Engeland, M. Hjorth-Jensen and E. Osnes, Nucl. Phys. **A634** (1998) 41.
- [62] B. Fogelberg and J. Blomqvist, Phys. Lett. **B137** (1984) 20
- [63] R.R. Whitehead, A. Watt, B.J. Cole and I. Morrison, Adv. Nucl. Phys. **9** (1977) 123.
- [64] T. Engeland, M. Hjorth-Jensen, A. Holt and E. Osnes, Phys. Scripta **T56** (1995) 58.
- [65] National Nuclear Data Center, Brookhaven National Laboratory.
- [66] D. Lu, G. He and R.H. Landau, Comp. Phys. Com. **108** (1997) 75.
- [67] M. Hjorth-Jensen, in preparation.
- [68] C. Mahaux and R. Sartor, Phys. Rep. **211** (1992) 53.
- [69] C. Mahaux, P.F. Bortignon, R.A. Broglia and C.H. Dasso, Phys. Rep. **120C** (1985) 1.
- [70] M.W. Kirson and L. Zamick, Ann. Phys. **60** (1970) 188.
- [71] F.L. Goodin and P.J. Ellis, Nucl. Phys. **A334** (1980) 229.
- [72] W.H. Dickhoff and H. Müther, Nucl. Phys. **A473** (1987) 394 and references therein.
- [73] K.L. Kowalski, Phys. Rev. Lett. **15** (1965) 798.
- [74] A. Nogga, D. Hüber, H. Kamada, and W. Glöckle, Phys. Lett. **B411**, (1997).
- [75] A. Akmal, V.R. Pandharipande and D.G. Ravenhall, Phys. Rev. **C58** (1998) 1804.
- [76] L. Engvik, M. Hjorth-Jensen, R. Machleidt, H. Müther and A. Polls, Nucl. Phys. **A627** (1997) 125.
- [77] H.Q. Song, M. Baldo, G. Giansiracusa, and U. Lombardo, Phys. Rev. Lett. **81**, (1998) 1584; Phys. Lett. **B411** (1997) 237; M. Baldo (private communication).
- [78] V.G.J. Stoks, R.A.M. Klomp, C.P.F. Terheggen and J.J. de Swart, Phys. Rev. **C49** (1994) 2950.
- [79] R.B. Wiringa, V.G.J. Stoks and R. Schiavilla, Phys. Rev. **C51** (1995) 38.
- [80] B.S. Pudliner, A. Smerzi, J. Carlson, V.R. Pandharipande, S.C. Pieper and D.G. Ravenhall, Phys. Rev. Lett. **76** (1996) 2416.
- [81] T. Engeland and M. Hjorth-Jensen, in preparation.



a



b



Folded